Landscape evolution, post-LGM surface denudation and soil weathering processes from Dickinson Park mire, Wind River Range, Wyoming (USA)

Egli, Markus ; Dahms, Dennis ; Dumitrescu, Mike ; Derakhshan-Babaei, Farzaneh ; Christl, Marcus ; Tikhomirov, Dmitry

Abstract: At mid-latitudes, the transition from the Pleistocene to the Holocene was characterised by distinct and partially abrupt climatic changes. Also during the Holocene, climatic perturbations, with sometimes cold-dry conditions, have occurred. How land surfaces and soil development processes in high-mountains respond to these climatic oscillations is so far only poorly known. We traced the responses of surfaces in the alpine settings of the Wind River Range (Wyoming, US) by using a large mire as natural archive. This enabled us to reconstruct environmental conditions and ecosystem changes during the Holocene in this montane area. Although adjacent moraine deposits display 10Be exposure ages from the Last Glacial Maximum up to MIS16 or even older, the accessible sediment deposits covered only the Holocene (via radiocarbon dating). By applying a geoforensic approach and deriving sedimentation rates, major climatic signals were detected. A higher deposition (and consequently erosion) rate and thus a higher rate of geomorphic activity was measured for the known cold periods 9.4–10.2 ka BP, 4.2 ka BP and 2.5 ka BP. During the LIA, especially rapid aggradation of organic matter organic matter took place here. Rates of chemical weathering and soil formation seem to have been relatively low until about 5–6 ka BP but have since increased during the Late Holocene. This would fit previous observations of increasing moisture conditions after the mid-Holocene aridity period. In contrast to several other studies, no clear signs of major disturbances (erosion, weathering) during the 8.2 ka event could be observed. Together with the low levels of chemical weathering found here, we do not see any evidence that the climate was more humid during this period. Compared to previous findings, more humid conditions seemed to have returned earlier, i.e. about 5 kyr BP. In general, this landscape displayed a patchy pattern of reaction to environmental changes, as all events were not recorded in each mire profile.

DOI: https://doi.org/10.1016/j.geomorph.2020.107433

Egli, Markus; Dahms, Dennis; Dumitrescu, Mike; Derakhshan-Babaei, Farzaneh; Christl, Marcus; Tikhomirov, Dmitry (2020). Landscape evolution, post-LGM surface denudation and soil weathering processes from Dickinson Park mire, Wind River Range, Wyoming (USA). Geomorphology, 371:107433.
DOI: https://doi.org/10.1016/j.geomorph.2020.107433

Geomorphology 371 (2020) 107433

Contents lists available at ScienceDirect

Geomorphology

journal homepage: www.elsevier.com/locate/geomorph

Landscape evolution, post-LGM surface denudation and soil weathering processes from Dickinson Park mire, Wind River Range, Wyoming (USA)

Markus Egli [a,*], Dennis Dahms [b], Mike Dumitrescu [a], Farzaneh Derakhshan-Babaei [c], Marcus Christl [d], Dmitry Tikhomirov [a,d]

[a] Department of Geography, University of Zürich, CH-8057 Zürich, Switzerland
[b] Department of Geography, University of Northern Iowa, Cedar Falls, USA
[c] Department of Physical Geography, Shahid Beheshti University (SBU), 1983969411 Tehran, Iran
[d] Institute of Ion Beam Physics, ETH-Zürich, CH-8093 Zürich, Switzerland

ARTICLE INFO

Article history:
Received 12 June 2020
Received in revised form 8 September 2020
Accepted 14 September 2020
Available online 16 September 2020

Keywords:
Erosion
Climate
Wind River Mountains
Landscape evolution

ABSTRACT

At mid-latitudes, the transition from the Pleistocene to the Holocene was characterised by distinct and partially abrupt climatic changes. Also during the Holocene, climatic perturbations, with sometimes cold-dry conditions, have occurred. How land surfaces and soil development processes in high-mountains respond to these climatic oscillations is so far only poorly known. We traced the responses of surfaces in the alpine settings of the Wind River Range (Wyoming, US) by using a large mire as natural archive. This enabled us to reconstruct environmental conditions and ecosystem changes during the Holocene in this montane area. Although adjacent moraine deposits display ^{10}Be exposure ages from the Last Glacial Maximum up to MIS16 or even older, the accessible sediment deposits covered only the Holocene (via radiocarbon dating). By applying a geoforensic approach and deriving sedimentation rates, major climatic signals were detected. A higher deposition (and consequently erosion) rate and thus a higher rate of geomorphic activity was measured for the known cold periods 9.4–10.2 ka BP, 4.2 ka BP and 2.5 ka BP. During the LIA, especially rapid aggradation of organic matter organic matter took place here. Rates of chemical weathering and soil formation seem to have been relatively low until about 5–6 ka BP but have since increased during the Late Holocene. This would fit previous observations of increasing moisture conditions after the mid-Holocene aridity period. In contrast to several other studies, no clear signs of major disturbances (erosion, weathering) during the 8.2 ka event could be observed. Together with the low levels of chemical weathering found here, we do not see any evidence that the climate was more humid during this period. Compared to previous findings, more humid conditions seemed to have returned earlier, i.e. about 5 kyr BP. In general, this landscape displayed a patchy pattern of reaction to environmental changes, as all events were not recorded in each mire profile.

1. Introduction

The Lateglacial-to-early Holocene transition was a period during which abrupt climate and environmental changes occurred worldwide (e.g., Alley and Vlark, 1999; Shakun and Carlson, 2010; Krause and Whitlock, 2013; Yu and Eicher, 2019). In the western US, regional climates shifted from full glacial conditions to the summer insolation maximum of the early Holocene (Krause et al., 2015). In the Pacific Northwest of North America, Osborn et al. (2012) report that a number of Holocene (Neoglacial) advances occurred during several distinct climate oscillations (at 2.2, 1.6, 0.9 and 0.4 ka). Lateral and end moraines, however, provided evidence for only one Holocene glacial event (LIA, 0.4 ka) following the Lateglacial Younger Dryas interval (12.6–11.7 ka).

In British Columbia, glacial advances continued into coastal areas such as the Fraser River valley until about 10 ka BP. The ice in the major valleys down-wasted after about 14 ka BP (Harris, 2019). However, at least one glacier or group of glaciers was advancing in each millennium of the Holocene in some area of northern British Columbia or Alaska indicating that climate oscillations continued to occur (Harris, 2019). Furthermore, it is well documented that major climatic changes have occurred at roughly 4.2 and 8.4 ka BP (Magny, 2004; Berger and Guilaine, 2009; Brisset et al., 2013). The 8.2 ka event was a period of abrupt cooling of 1–3 °C across large parts of the Northern Hemisphere, which lasted for about 160 yr (Matero et al., 2017). Although the 4.2 ka event gave rise to an abrupt climate change with either dry or wet and cool climatic conditions (Ran and Chen, 2019) in many parts of the world, a review of paleoceanographic and terrestrial paleoclimatic

* Corresponding author.
E-mail address: markus.egli@geo.uzh.ch (M. Egli).

https://doi.org/10.1016/j.geomorph.2020.107433

data from around the northern North Atlantic revealed no compelling evidence for a significant climatic anomaly in this region (Bradley and Bakke, 2019). Although these cold events were not always related to major glacial advances, they seemed to have had, nonetheless, major impacts on vegetation and in general on the environment (Engel et al., 2010; Malkiewicz et al., 2016; Boxleitner et al., 2017). Shuman and Serravezza (2017) found evidence that climatic conditions varied relatively distinctly even in the Early Holocene. They compared the stratigraphic correlations among several lake sediment cores in Wyoming and Colorado and found widespread evidence for a Terminal Pleistocene Drought from 15 to 11 ka BP, an early Holocene humid period from 11 to 8 ka BP, and mid-Holocene aridity from 8 to 5.5 ka BP. By comparing these lake records with the regional literature, the following patterns were identified: i) an extensive drying in the western US after 15 ka BP; ii) regional differences during the Pleistocene-Holocene transition, including enhanced runoff derived from Pacific storms; 3) increasing insolation anomalies giving rise to a north-south contrast from 9 to 6 ka BP that is consistent with a northward shift in storm tracks; and 4) rapid increases in effective moisture across much of western North America from 6 to 4 ka (Shuman and Serravezza, 2017).

Mountain ranges are, obviously, very geomorphologically active regions. Surface erosion by mass movements, snow avalanches, mudflows or solifluction are important processes (among many others) in such areas. Changing climatic conditions raise questions about the co-evolution of landscapes and their associated soils. So far, it is only poorly known how surface processes in high-mountain areas, including erosional processes and soil formation, may have reacted to the previously-noted climatic oscillations. This raises the question of how landscapes and their soils co-evolve in mountain regions and how they are related to climate change. Harrison et al. (2019) demonstrate that climate changes may result in highly differentiated and nonlinear landscape response that are sensitive to antecedent conditions, autogenic properties and processes. The existing knowledge in this research is still incomplete and fragmented.

With the help of mires, details of changes in climates of the past can be reconstructed. Mires are important natural archives when it comes to reconstructing climate, environmental and ecosystem changes (Lamentowitcz et al., 2015; Boxleitner et al., 2017). The main aim of our study was consequently to trace surface processes and identify any erosional phases and intervening stable periods and their relations to soil formation in a montane region of the Wind River Range as a function of changing climatic conditions. We selected a mire as our primary environmental archive and associated soils in the surrounding landscape through the use of a geochemical approach ('geoforensics'). The main research questions were: how did the landscape surrounding the mire react to climatic oscillations? When do erosional phases predominate versus stable periods with soil formation? We hypothesised that: 1) soil formation (progressive phases) and erosion (regressive phases) should be recorded through changes in geochemical signatures in the mire, 2) these can be correlated to climatic conditions and that 3) the mountain environment of the Wind River Range reacted sensitively towards local/regional climatic oscillations.

2. Study site and sampling strategy

2.1. Study site

The glacial history of the Wind River Range of Wyoming (USA) is mapped and relatively well dated (Dahms et al., 2010, 2018). Dahms et al. (2018) recently demonstrated that moraines of the central Rocky Mountains (Wind River Range, Wyoming, USA) that previously were identified as mid-Holocene and Younger Dryas-age allostratigraphic units showed equivalence to only Lateglacial events: 17.5–14.7 ka, just prior of the Bølling interstadial and to 13.9–11.7 ka, the Intra-Allerød Cold Period-Younger Dryas stadial phase. They concluded, therefore, that little evidence exists for early to middle Holocene cool climate events in the southern Wind River Range, which may correspond to major climatic and environmental shifts at the Late Pleistocene to Early Holocene transition. Moraine evidence, however, still exists in the WRR for two Late Holocene glacial advances: the Gannett Peak and Black Joe allostratigraphic units. These are thought to correspond to the Little Ice Age (LIA) and a slightly earlier undated cold period, respectively (Dahms, 2002; Dahms et al., 2010).

The Wind River Range (WRR) is located in the Middle Rocky Mountains of west-central Wyoming (Fig. 1). The range is a Laramide-age structure (~ 60 Ma) uplifted along the generally NW-SW–trending Wind River thrust fault (Brewer et al., 1982). The uplift tilted the Paleozoic and Mesozoic sedimentary cover to the east where subsequent erosion exposed the Precambrian crystalline core of the range over an area 175 km long by 45 km wide and created a series of hogbacks and canyons in the Paleozoic/Mesozoic sedimentary units along the east flank of the range (Steidtmann et al., 1989). Bedrock of the range core in the study area is mostly Archaean granite and granodiorite of the Louis Lake Formation (Love and Christianson, 1985; Frost et al., 2000).

The Wind River Range has a relatively high density of wetlands (Copeland et al., 2010). Since the range was in the past strongly influenced by glaciers, the water from present-day glaciers and snow fields now collects into an impressive collection of palustrine, riverine and lacustrine features (Heidel, 2013). Thus, we should be able to find ideal settings that reflect the relations between the glacial and environmental history of the Wind River Range (WRR). To trace surface processes and their relations to climatic oscillations, we investigated a mire in Dickinson Park on the south-eastern slope of the range (Fig. 1). Dickinson Park is a remote area in the Shoshone National Forest at an altitude of about 2843–2852 m a.s.l. Mean annual precipitation and temperature here, as recorded at the nearby Hobbs Park, Wyoming NRCS-USDA SNOTEL locality from 1979 to 2020 is 713 mm yr^{-1} and 0.5 °C (https://www.nrcs.usda.gov/wps/portal/wcc/home/quicklinks/imap). The mire has an area of about 0.8 km^2. The mire is fed by small creeks at its western end. The mire lies on a plateau in the lower third of the long (about 27 km) and formerly glaciated valley of the North Fork (Popo Agie) river (Fig. 2a). The catchment of the mire is about 9.1 km^2. The average slope at the lower elevations is between 5 and 15% and at higher elevations usually about 20 to 25%. The altitudinal range of Dickinson Park is between 2843 and 3357 m a.s.l. (Fig. 2c, d).

2.2. Sampling strategy

We chose the best positions for drilling using avalanche probes to find the thickest and presumably oldest layers in the mire for sampling (cf. Boxleitner et al., 2017). In total, 5 cores were taken from the mire (Fig. 2b). Cores were drilled to refusal at all sites (max. depth of 650 cm; profile 3b). Initial sampling was done to ~2 m using a Russian side-opening sampler (core 1). Due to the inter-bedding of more sandy sediments with the organic layers, we used a Vibra-Corer to reach greater depths (to 6.5 m, core 3b). The Vibra-Corer apparatus combines a 5 cm-diameter Livingston corer with a concrete vibrator to force the core barrel through the coarse sandy sediments.

In order to relate the mire core sediments to the local landscape processes, we sampled 5 soil profiles on the backslopes and footslopes of the moraine and sediment complex enclosing the mire. The soil profiles were excavated to the BC or C horizons and samples taken based on the horizon designation. By using the chemical signatures of these soil horizons and comparing them to the mire profiles, the origin of the sedimented material should be better traceable and attributable to the general geomorphic events of erosion and deposition. We assumed that most of the deposited material in the mire stems from surface-wash. Therefore, soil erosion, surface denudation or maybe shallow landslides can be expected. Evidence of debris flow was not recognisable although they may exist at higher altitudes of the catchment. Fig. 3 gives an impression of the present-day situation of the

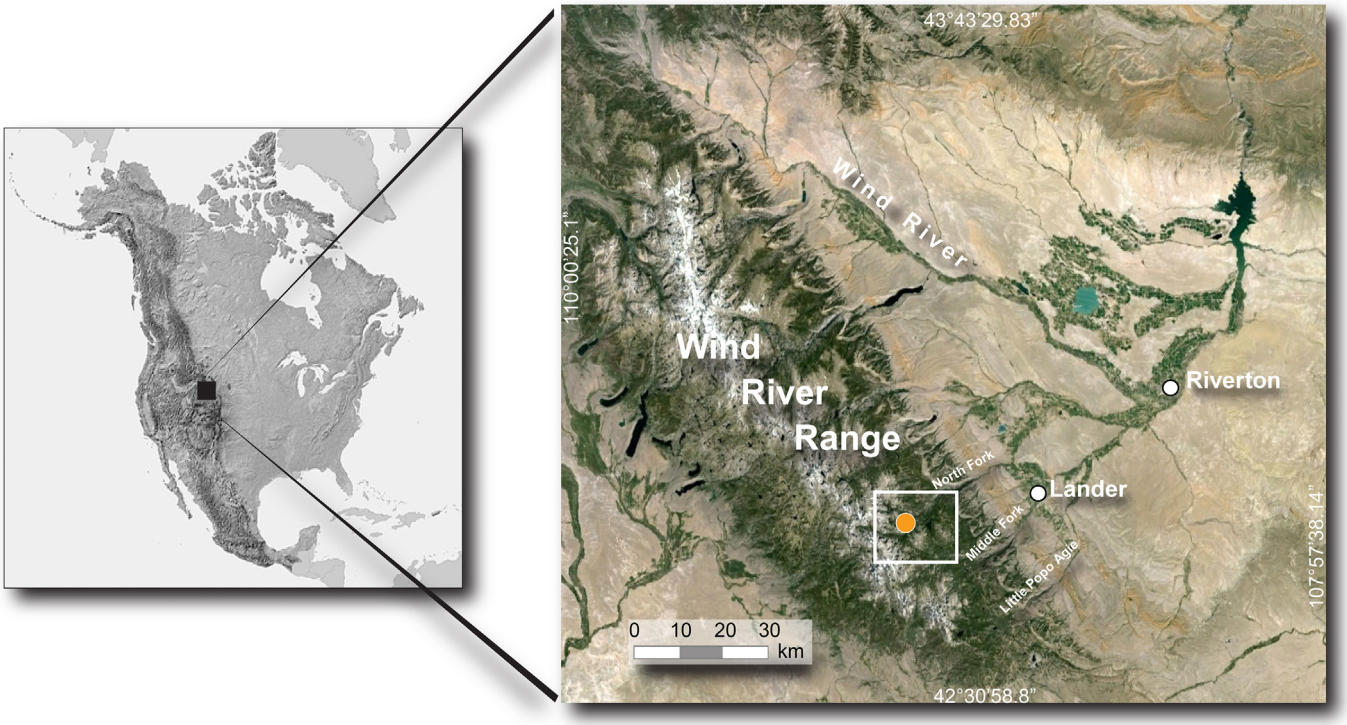

Fig. 1. Location of the Dickinson Park study area of the North Fork valley in the Wind River Range (Wyoming, USA; Google Earth image; Dahms et al., 2018).

mire with views to the west (Fig. 3a) and east (Fig. 3b) and of the sampled soils.

To constrain the age of the landscape contributing sediments to the mire we sampled a number of boulders on the adjacent moraine complex for ^{10}Be exposure dating. To obtain the most reliable exposure ages, we used commonly-accepted methods for sampling moraine boulders (e.g., Gosse and Phillips, 2001; Masarik and Wieler, 2003). We chose large, high (2–5 m) boulders on landscape positions where we could reasonably rule out post-depositional tilting. These boulders were sampled on their relatively flat tops in an attempt to avoid edge effects.

3. Material and methods

3.1. Mire core and soil sample preparation and analysis

The mire cores were sub-sampled at 10 cm intervals, accounting for natural stratigraphic/sedimentary breaks. Samples from the mire cores and the soil samples were oven dried (at 70 °C), gently crushed and sieved at 2 mm to separate the fine earth fraction (<2 mm) from gravel (>2 mm). Soil pH (in 0.01 M $CaCl_2$) was determined on fine-earth samples using a soil:solution ratio of 1:2.5. Fe, Al and Mn concentrations were determined (in duplicate) after treatment with NH_4-oxalate (buffered at pH 3; McKeague et al., 1971). The extracts were centrifuged for 8 min at 4000 rpm and filtered through 0.45 μm mesh (S&S, filter type 030/20). Element concentrations were measured using atomic absorption spectroscopy (analytikjena contrAA 700). Element concentrations were furthermore controlled using standard addition (recovery ≥95%). The oxalate (Al_O, Mn_O, Fe_O) treatment extracts both the weakly- and poorly crystalline phases of these elements, as well as some of the organic phases. The method normally does not dissolve the strong humus-metal complexes (Mizota and van Reeuwijk, 1989). To determine the organic matter content, we performed loss on ignition (LOI) by igniting 2 g of oven-dried fine earth at 550 °C for 12 h. Measurement of the total element content of fine earth was done by means of X-ray fluorescence (XRF). Approximately 5 g of soil material was milled to <50 μm and analysed as loose powder in sample cups using an energy dispersive X-ray fluorescence spectrometer (SPECTRO X-LAB 2000, SPECTRO Analytical Instruments, Germany).

3.2. Mineralogy

For a general, qualitative overview of soil minerals present, we performed XRD (Bruker AXS D8 Advance, CuKα) and DRIFT (Diffuse Reflection Infrared Fourier Transform; Bruker, Tensor 27) measurements of the fine silt and clay fractions (< 32 μm). The DRIFT analyses done for both the soil and mire samples and were run from 250 to 4000 cm^{-1}. About 30 mg of finely-ground soil material and 270 mg of KBr were homogenised in a mill using a fine ball-mill (Zr) for 30 s at 10 rpm. Prior to measurement, the samples were dried in an oven at 70 °C for 2 h. The individual spectra were interpreted using OPUS 6 software. On selected samples, the clay mineral composition was determined in more detail. For this purpose, the clay fraction was extracted. Following a sequence of Mg saturation, glycerol solvation, K saturation and heating at 335 and 550 °C, specimens were oriented on glass slides and analysed using the procedures of Moore and Reynolds (1997) and Egli et al. (2001). We used a Rigaku SmartLab Automated Multipurpose X-ray Diffractometer equipped with a 3 kW sealed tube X-ray generator with a standard Cu target. Using Cu–Kα radiation generated at 40 kV and 30 mA, the slides were scanned from 3 to 15° 2θ with a step of 0.01° 2θ and a speed of 2° 2θ per minute.

3.3. Radiocarbon dating

The cleaned material (standard alkali-acid-alkali treatment) was combusted at 900 °C to produce CO_2 which was then reduced to graphite. The ratios of the carbon isotopes were measured by Accelerator Mass Spectrometry (AMS) using the 0.2 MV MICADAS facility at the Institute of Ion Beam Physics at the Swiss Federal Institute of Technology, Switzerland. The radiocarbon ages were calibrated with OxCal4.3 using IntCal13 (Reimer et al., 2013). Age-depth modelling was performed using the R-code 'clam' (Blaauw, 2010).

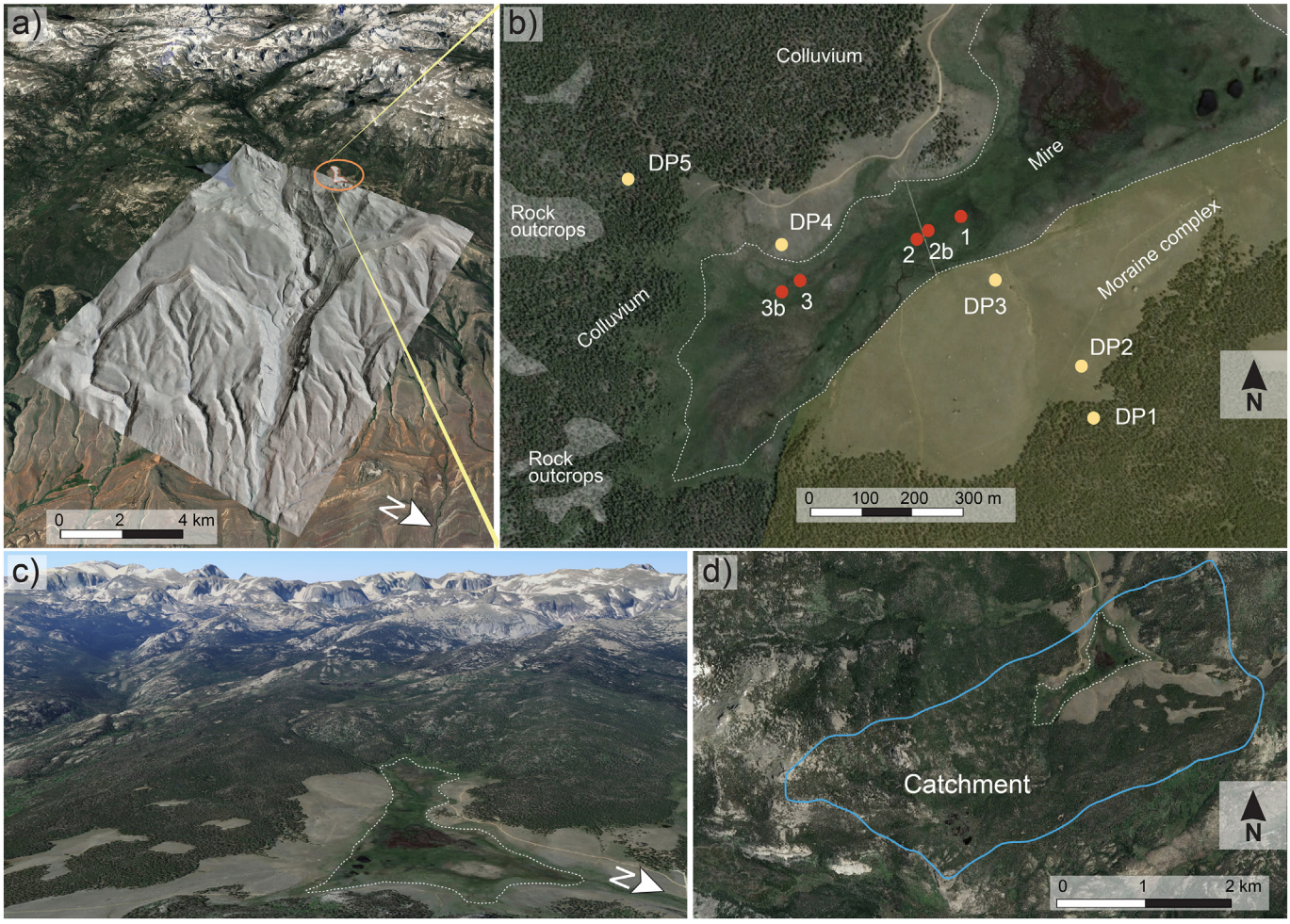

Fig. 2. a) View along the North Fork (Google Earth image) towards the mountain range and location of the investigated mire. The digital elevation model highlights the position of Dickinson Park relative to the adjacent glaciated canyon of the North Fork valley. b) View of the investigated mire profiles (red points) and investigated soils (DP1–5) (Google Earth image) with geomorphic units that surround the mire. c) Scenic view from the mire towards the crest of the WRR. d) Outline of the catchment of the mire.

3.4. Surface exposure dating

Shielding was measured for all boulders directly in the field. Extraction of ^{10}Be was processed at the University of Zurich including the following steps. The rock samples (~2 kg) were crushed and sieved to the 0.5–1 mm fraction. After having removed excess feldspar by froth flotation, the samples were leached for two weeks with a hydrofluoric acid (HF) solution on a shaker to obtain pure quartz. The further procedure to extract $Be(OH)_2$ is described in details in Dahms et al. (2018). All ^{10}Be/^{9}Be ratios were measured at the ETH Zurich AMS system Tandy accelerator (Christl et al., 2013) and normalised to the ETH in-house AMS standards S2007N and S2010N (^{10}Be/^{9}Be $= 28.1 \times 10^{-12}$ and 3.3×10^{-12} respectively) which have been calibrated to ICN 01-5-1 standard (Nishiizumi et al., 2007). All AMS standards are associated with a ^{10}Be half-life of 1.387 ± 0.012 Myr (Chmeleff et al., 2010). ^{10}Be/^{9}Be ratios were corrected to a preparation blank. ^{10}Be exposure ages were calculated using CRONUS-Earth (http://hess.ess.washington.edu/math/) version 3.0 (Table S1). The production rate, and thus the age, were scaled for latitude and altitude using the (Lal/Stone) time-dependent scaling scheme (Lal, 1991; Stone, 2000).

3.5. Weathering indices

Weathering indices are used to determine the degree of weathering of soils and sediments. We used the molar ratios of (Ca + K)/Ti to estimate the degree of weathering for the sediments. Our assumptions are that the lower the weathering ratio, the more advanced weathering is thought to be (Harrington and Whitney, 1987).

Meunier et al. (2013) proposed an additional index to trace chemical weathering that not only takes the decreasing amounts of alkali-alkaline earth and divalent metallic components into account, but also considers the content of trivalent chemical components (R^{3+}). Meunier's weathering intensity scale (WIS) is given by:

$$WIS = \frac{R^{3+}}{\left(M^{+} + R^{2+} + R^{3+}\right)} \quad (1)$$

with $R^{3+} = Al^{3+} + Fe^{3+}$; $R^{2+} = Mg^{2+} + Fe^{2+} + Mn^{2+}$ and $M^{+} = Na^{+} + K^{+} + 2Ca^{2+}$ (Meunier et al., 2013; Fang et al., 2019). Fe^{2+} is estimated using the oxalate-extractable content (that extracts weakly to poorly crystalline and organically-bound Fe^{2+} under reducing conditions in the mire). The M^{+}, 4Si and R^{2+} amounts are normalised to 100%. These values are used to calculate the Δ4Si where:

$$\Delta 4Si = \frac{[(4Si_{soil} - 4Si_{UCC}) \times 100]}{(100 - 4Si_{UCC})} \times 100 \quad (2)$$

$4Si_{UCC}$ corresponds to the upper continental crust (39.8%; Condie, 1993; Meunier et al. (2013)). The amount of 4Si corresponds to the number of Si^{4+} cations divided by 4 to refer to the general formula

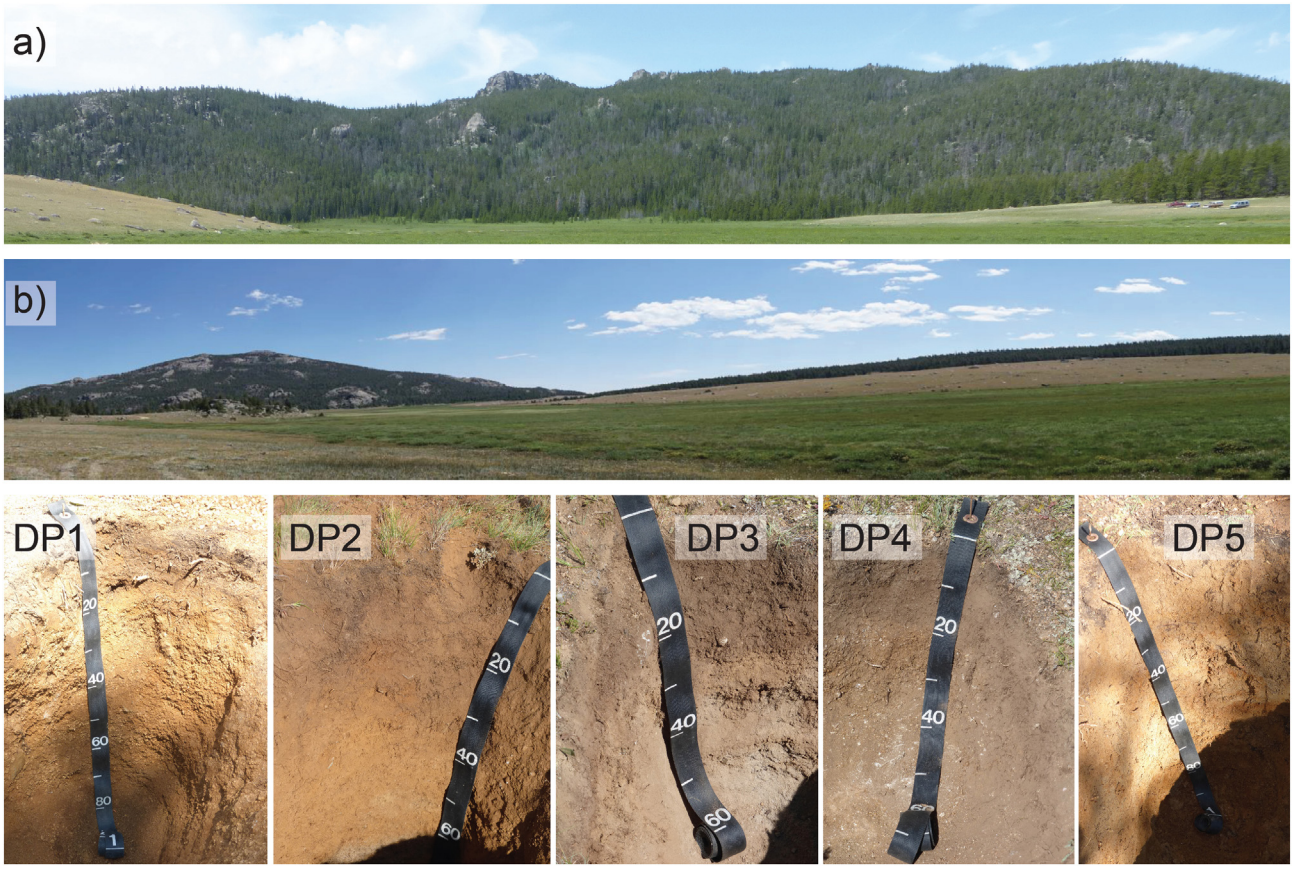

Fig. 3. a) View from the mire to the west; b) view across the mire to the east; DP1 – DP5 (cf. Fig. 2): profile photos of the investigated soil profiles.

unit of phyllosilicates. A higher Δ4Si denotes a higher degree of chemical weathering (as the more easily-weathered cations are sequentially removed). The maximum degree is reached when the parent rock is completely transformed into kaolinite (Δ4Si = 100; Fang et al., 2019).

4. Results

4.1. General context

The mire near Dickson Park is located next to a chronosequence of three/four left lateral moraines created by advances of the North Fork valley glacier and therefore holds some relation to these landforms (Figs. 2 and 4). Cosmogenic nuclide dating (^{10}Be) revealed ages between 537 and 17.8 ka (Table 1 and Fig. 4) when using a rock surface erosion of 1 mm per kyr^{-1}. With 2 mm erosion per kyr^{-1} for the oldest boulders, ^{10}Be indicates saturation and, thus, ages >1 Ma. These ages therefore confirm that this moraine complex was formed over several glacial periods ranging from at least MIS16 to MIS2. The area of the mire was ice-free during the LGM (Fig. 4).

4.2. Soils

The soils around the mire have developed on the moraine deposits (DP1, DP2, DP3) and on colluvial materials from the adjacent bedrock slopes (DP4, DP5) to the North and NW of the mire (Figs. 2 and 3). Profiles DP5 and DP1 are located in the surrounding forests, DP3 and DP4 are located close to the mires and DP2 is slightly more uphill. Profiles DP1, DP2 and DP3 are located on the moraine associated with the oldest boulder ^{10}Be ages (DIP-1, DIP-2). All five soil profiles have a typical structure with A horizons above Bw, Bt or Bg horizons over BC/CB or Cox horizons. The parent materials are either loamy sand or sandy loam (Table 2). The A and B horizons are mostly sandy loam to loam.

All soils are acidic (Table 2). In all soils, the highest pH values were measured in the A horizons, which is rather unusual and might indicate either erosional processes or some dust input (note the relatively high silt content of the upper horizons). The A horizons are relatively humus rich and org. C varied between 4.5% and 9%. Organic matter (LOI) strongly decreases with depth (Table 2).

Total elemental chemistry, DRIFT and XRD analysis reflect the granitic sources of the parent materials (Table 3). Typically, quartz and mica also are ubiquitous. Kaolinite, vermiculite, hydroxy-interlayered vermiculite (HIV) and mixed-layered minerals are the most common clay minerals present here (Table S2). The contents of oxalate-extractable Al, Fe, Mn and Si strongly decrease with soil depth with the exception of DP5 where the highest content was detected at greater depth (presumably due to redoximorphism and a lithological change; Table 2). Profiles DP2, DP3 and DP4 appear to show signs of erosion, as they are distinctly thinner than profiles DP1 and DP5.

4.3. Mire/sediment profiles

The mire profiles have an organic rich layer to a maximum depth of about 2 m (Fig. 5). This organic rich layer is sometimes intercalated with gravel deposits. The greatest drilling depth was achieved at profile 3b; however, the largest part of this profile consists of gravel deposits with small amounts of organic matter. A total of 14 samples were successfully dated from the five mire cores (Table 4). A maximum age of 10,245–10,188 calBP was obtained from a depth of 465 cm in profile 3b. The age trends of profiles 1, 2 and 3b are similar to a depth of 1 m (Fig. 6). Only profile 3 exhibits a stronger age/depth profile. Here, an age of about 10 ka is reached near 1 m. Profiles 1, 2 and 3b, show a

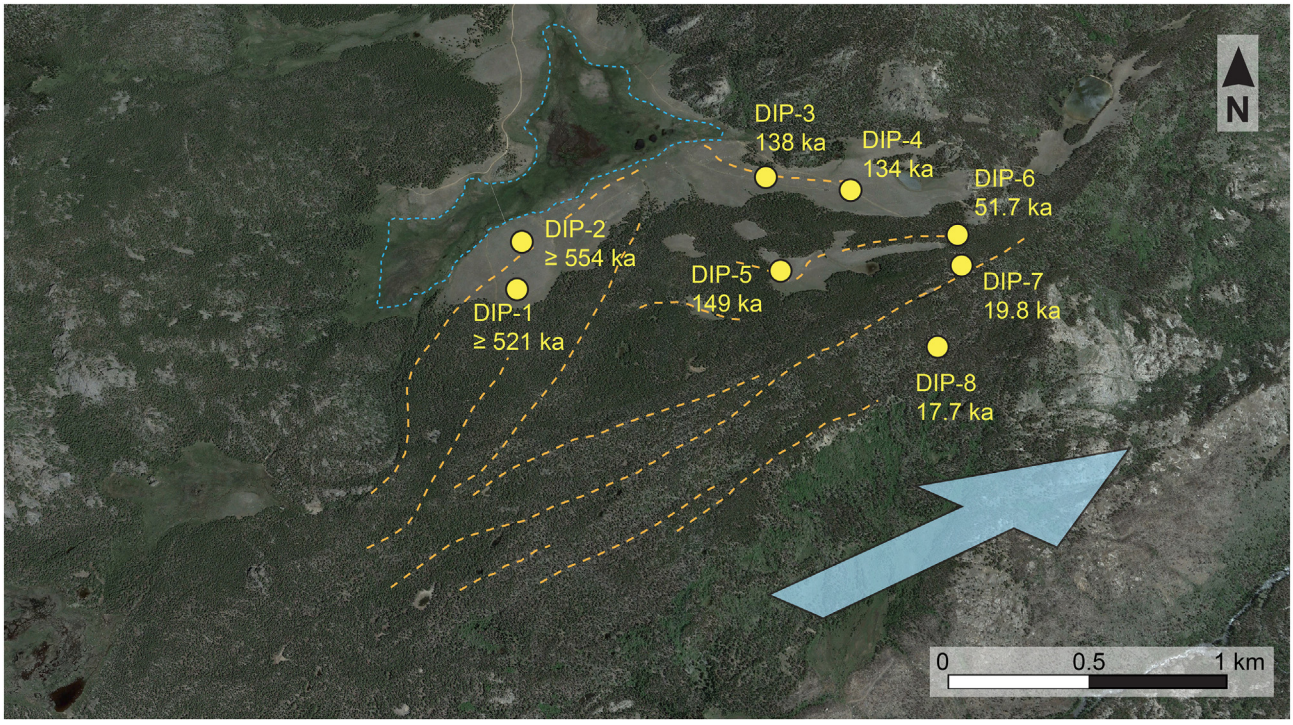

Fig. 4. Surface exposure ages of boulders on the moraine complex constraining the mire. The blue arrow indicates the flow direction of the former glacier (Google Earth image), the blue dotted line the present-day extension of the mire and the dashed yellow line presumed moraine ridges.

clear change at 1–1.5 m. Profiles 3 and 3b have a considerably higher pH value than profiles 1 and 2 (Fig. 7). In addition, the pH values increase with depth at profile 3 and 3b from values slightly less than 5 up to 6.5. The onset of organic C accumulation is different among the profiles. Profile 3 shows a strong OC accumulation for about the last 8 kyr whereas OC accumulation began about 4 kyr ago in profiles 1, 2 and 3b (Fig. 7). The organic matter content (as carbon sequestration) decreased in profiles 1 and 2 between about 2000 to 100 BP.

Similar to the pH trends, we detect a distinct difference between profiles 1, 2, and 3 and 3b. Note that the LOI contents in profiles 3 and 3b are nearly 80%, whereas LOI in the other cores reached only to about 40%. This suggests that more inorganic material is accumulating and being admixed into the upper layers of profiles 1 and 2. LOI is a commonly accepted method, but it may include also some hydrated compounds from mineral structural water. Usually, the higher the LOI the lower is the proportion of mineral structural water (Sun et al., 2009).

The (Ca + K)/Ti ratios of profile 3b exhibit a distinct change with increasing age towards lower values (Fig. 8a) which indicates either stronger chemical weathering conditions or a change in the origin of the deposited material. We find the same trend along profile 2b. There, too, strong fluctuations begin >4000 calBP. At ages <4000 calBP the ratio remains quite stable (between 5 and 10) in profiles 1 and 2. Profiles 3 and 3b again show a distinct trend with increased age. The ratio is >15 until about 4000–6000 BP and lowers into the range near the other profiles after 4000 BP. The (Ca + K)/Ti ratio is considerably lower with ages >4000 calBP. As an average, the (Ca + K)/Ti ratio are in the range of what is measured in the soils (Fig. 8). However, the profiles 3 and 3b are sometimes distinctly outside this range.

K/Rb and Ti/Zr ratios are commonly applied to determine changes in lithogenic sources (Silva-Sánchez et al., 2015; Fig. 8b, c). Rb is strongly linked to K, whereby Rb bonds more strongly to silicates than with K (Kabara-Pendias and Pendias, 2000). Therefore the K/Rb ratio can indicate the presence of weathering processes because it decreases during soil formation. Similar to the (Ca + K)/Ti ratio, an increasing variability can also be seen in profile 2 during 4000–5000 BP (Fig. 8b). In profile 3b we see extreme fluctuations over the entire depth of the core. The values generally increase with decreasing depth upward towards the surface.

The phenomenon of high ratio fluctuations around 4000 years BP, as previously seen with the two other indices, is also reflected in the Ti/Zr

Table 1
Exposure ages of moraine boulders, Dickinson Park, using the Lm time dependent scaling scheme.

Sample	Latitude (°N)	Longitude (°E)	Elevation (m a.s.l.)	Sample thickness (cm)	Shielding factor	Erosion rate (mm ky^{-1})	10Be content (x10^5 atoms g^{-1})	^{10}Be Exp Age (ka)[b]	^{10}Be Exp Age (ka) (erosion rate = 2 mm ky^{-1})
DIP-1	42.824	−109.056	2880	2.0	0.997	1.00[a]	113.29 ± 3.80	520.7 ± 79.7 (32.5)	Saturated[a]
DIP-2	42.825	−109.056	2882	2.0	0.999	1.00[a]	116.27 ± 3.73	554.1 ± 84.8 (33.3)	Saturated[a]
DIP-3	42.828	−109.045	2870	2.0	0.998	1.00	42.78 ± 1.38	137.6 ± 13.1 (5.2)	
DIP-4	42.827	−109.041	2873	2.0	0.997	1.00	41.80 ± 1.34	133.8 ± 12.7 (5.0)	
DIP-5	42.824	−109.044	2901	2.0	1.000	1.00	46.70 ± 1.56	149.1 ± 14.5 (5.9)	
DIP-6	42.825	−109.036	2913	2.0	0.998	1.00	17.60 ± 0.60	51.7 ± 4.5 (1.9)	
DIP-7	42.824	−109.037	2919	2.0	1.000	1.00	6.88 ± 0.27	19.8 ± 1.7 (0.8)	
DIP-8	42.822	−109.040	2929	2.0	0.852	1.00	5.24 ± 0.22	17.7 ± 1.6 (0.8)	

[a] Erosion rates of up to 2 mm/ky for older Pleistocene deposits (Dahms et al., 2018).
[b] Age with external and internal uncertainty (1-sigma).

Table 2
Typical chemical and physical properties of the soils adjacent to the mire.

Location, elevation (m a.s.l.)	Horizon	Depth (cm)	Gravel wt.-%	Gravel vol.- %	pH ($CaCl_2$)	Al(o) mg/kg	Mn (o) mg/kg	Fe(o) mg/kg	Si(o) mg/kg	N (%)	C (%)	C/N	LOI (%)	Particle size distribution (%)			Bulk density (g cm^{-3})
														Sand[a]	Silt	Clay	
DP1	A	0–10	6	2	4.55	4773	1314	5969	488	0.25	4.50	17.9	13.3	50	42	8	0.7
2886	Bw1	10–30	37	22	4.25	3402	97	5428	361	0.07	0.92	14.0	6.1	50	34	16	1.3
	Bw2	30–85	66	57	4.38	2216	70	1334	378	0.01	0.18	17.0	2.2	84	11	5	1.8
	Cox	85+	67	59	4.50	1688	164	1347	233	0.01	0.14	13.0	2.1	84	13	4	1.9
DP2	A	0–2	34	19	5.31	1855	511	4239	270	0.53	7.10	13.5	16.9	59	30	11	1.2
2870	BA	2–15	24	17	4.92	2031	247	4398	550	0.28	3.08	11.1	9.0	62	24	15	1.7
	Bw1	15–30	35	28	4.50	2034	31	3013	359	0.13	1.33	10.4	5.7	68	19	13	1.9
	Bw2	30–53	39	31	4.30	1694	68	3478	204	0.05	0.63	11.9	4.8	70	18	13	1.9
	Bt	53–60	34	29	4.21	1048	65	1551	93	0.02	0.28	14.9	2.6	77	12	11	2.1
	Cox	60+	41	36	4.24	627	43	895	65	0.01	0.17	13.2	1.8	71	22	7	2.1
DP3	A	0–10	24	12	5.30	1835	309	3036	389	0.43	4.89	11.5	12.2	53	31	16	1.1
2858	Bw	10–25	40	27	4.94	1995	138	1834	332	0.18	2.11	12.0	6.2	66	23	11	1.5
	BC	25–45	36	29	4.79	1363	61	1076	216	0.10	1.20	12.6	4.3	71	18	11	1.9
	Cox	45+	43	37	4.92	326	31	304	36	0.01	0.18	13.1	0.9	80	18	2	2.1
DP4	A	0–7	27	13	5.31	1488	497	3016	238	0.54	6.36	11.7	13.2	55	32	12	1.1
2865	AB	7–20	38	23	4.95	1529	387	2373	1259	0.18	2.01	11.0	6.0	56	30	15	1.3
	2Bw	20–45	61	47	5.07	820	39	593	43	0.07	0.42	6.4	4.6	78	9	13	1.5
	2BC	45+	30	20	4.97	745	54	313	29	0.04	0.80	21.8	5.7	72	16	13	1.5
DP5	OA	0–4	9	3	4.92	1745	616	2925	423	0.40	8.95	22.2	19.7	51	35	14	0.9
2883	Bw	4–20	18	11	4.51	783	12	2801	87	0.03	0.53	15.3	3.4	70	20	10	1.5
	2Bg	20–90	3	1	4.52	1241	5	3234	231	0.04	0.49	11.6	6.1	43	39	18	1.1
	2CBg	90–100+	26	21	4.84	771	54	4174	236	0.02	0.30	15.2	3.9	67	22	11	2.0

[a] Sand: 2–0.5 mm; Silt: 500–2 μ; Clay: <2 μm.

ratio, but these fluctuations cannot be detected in profile 3. Here the values increase continuously with depth. Profiles 3 and 3b exhibit values that are mostly outside the range of the adjacent soils.

When viewing these indices, we can again distinguish profiles 3 and 3b from profile 1 and 2 (Fig. 9). Profile 3 and 3b clearly exhibit a lower degree of weathering than the other (Fig. 9c). While the WIS or Δ4Si values generally decreased during the last 4 kyr at the profiles 3 and 3b, a contrasting trend exists for profiles 1 and 2. In general, the profiles 1 and 2 are closer to the kaolinite and Al- and Fe-oxyhydroxides corner of the diagram.

Some slightly contrasting results are seen in the oxalate-extractable fractions of Al and Fe (Fig. 10). The Al(o) content remains high or increases in all profiles, even during the last 4 kyr. A strong increase in Fe(o) is seen in profiles 1 and 2, while Fe(o) remained low in 3 and 3b, but nonetheless exhibited an increase during the last 3–4 kyr.

Based on the age/depth trends of the mire, we can calculate a yearly sedimentation rate. The sedimentation rate increased strongly over time in profiles 1 and 2 (Fig. 11). Using a linear interpolation between the ^{14}C dates, the profiles exhibit major peaks in sedimentation rates about 9–10 ka, 4.2 ka, 2.3 ka BP and for the last ca. 400 years. These increased sedimentation rates cannot be identified simultaneously at all sites. In addition, profile 3b shows a slight increase in sedimentation rate from about 6–8 kyr BP.

5. Discussion

5.1. Glacier dynamics

The large moraine complex enclosing the Dickinson Park mire is composed of lateral moraines representing several Middle- to Late

Table 3
Total contents of some major elements in the soils.

	Horizon	Depth range	Na	Mg	Al	Si	K	Ca	Ti	Mn	Fe	Zr
		cm	%	%	%	%	%	%	%	%	%	%
DP-1 A	A	0–10	1.28	1.07	6.59	26.23	2.05	0.87	0.417	0.170	2.92	0.025
DP-1 Bw1	Bw1	10–30	1.32	1.06	7.47	28.09	2.26	0.76	0.415	0.035	2.87	0.022
DP-1 Bw2	Bw2	30–85	1.86	0.88	7.13	29.93	2.70	1.16	0.314	0.027	2.24	0.016
DP-1 BC	Cox	85+	2.06	0.76	6.99	31.38	2.98	1.26	0.287	0.035	1.71	0.014
DP-2 A	A	0–2	1.56	0.75	5.35	25.68	2.42	1.16	0.286	0.075	2.18	0.019
DP-2 BA	BA	2–15	1.79	0.75	6.19	28.99	2.42	1.24	0.335	0.050	2.68	0.023
DP-2 Bw1	Bw1	15–30	1.59	1.00	6.91	27.62	2.11	1.17	0.387	0.033	3.54	0.031
DP-2 Bw2	Bw2	30–53	1.75	0.97	7.07	29.41	2.19	1.32	0.389	0.031	3.30	0.031
DP-2 Bt	Bt	53–60	1.72	1.00	7.16	28.85	2.16	1.42	0.467	0.032	3.83	0.048
DP-2 Cox	Cox	60+	2.01	1.06	6.76	29.70	2.37	1.66	0.475	0.029	3.12	0.039
DP-3 A	A	0–10	1.68	0.84	5.86	27.88	2.30	1.33	0.332	0.056	2.70	0.024
DP-3 Bw	Bw	10–25	1.85	0.80	6.17	29.79	2.37	1.48	0.400	0.038	2.97	0.031
DP-3 BC	BC	25–45	2.01	0.94	6.63	30.54	2.33	1.59	0.411	0.031	3.29	0.034
DP-3 Cox	Cox	45+	2.65	0.59	6.76	37.17	3.01	2.01	0.381	0.025	3.14	0.045
DP-4 AB (Bw1)	A	0–7	1.41	1.01	5.82	25.38	2.04	1.26	0.328	0.086	2.51	0.021
DP-4 2 Bw	AB	7–20	1.52	1.05	6.70	27.80	2.12	1.13	0.395	0.068	2.89	0.029
DP-4 2 Bw	2Bw	20–45	1.86	1.46	7.84	26.20	1.78	1.51	0.476	0.039	4.07	0.041
DP-4 2 BC	2BC	45+	1.65	1.42	8.04	27.37	1.45	1.48	0.312	0.029	2.60	0.022
DP-5 OA	OA	0–4	1.58	1.06	5.41	23.56	1.68	1.41	0.361	0.092	2.56	0.029
DP-5 Bw	Bw	4–20	1.70	1.30	6.93	28.79	1.98	1.56	0.485	0.034	3.39	0.036
DP-5 2Bg	2Bg	20–90	1.33	1.41	7.25	28.18	1.95	1.13	0.497	0.028	3.30	0.030
DP-5 2 CBg	2CBg	90–100+	1.65	1.49	7.08	28.00	1.86	1.59	0.461	0.034	4.00	0.032

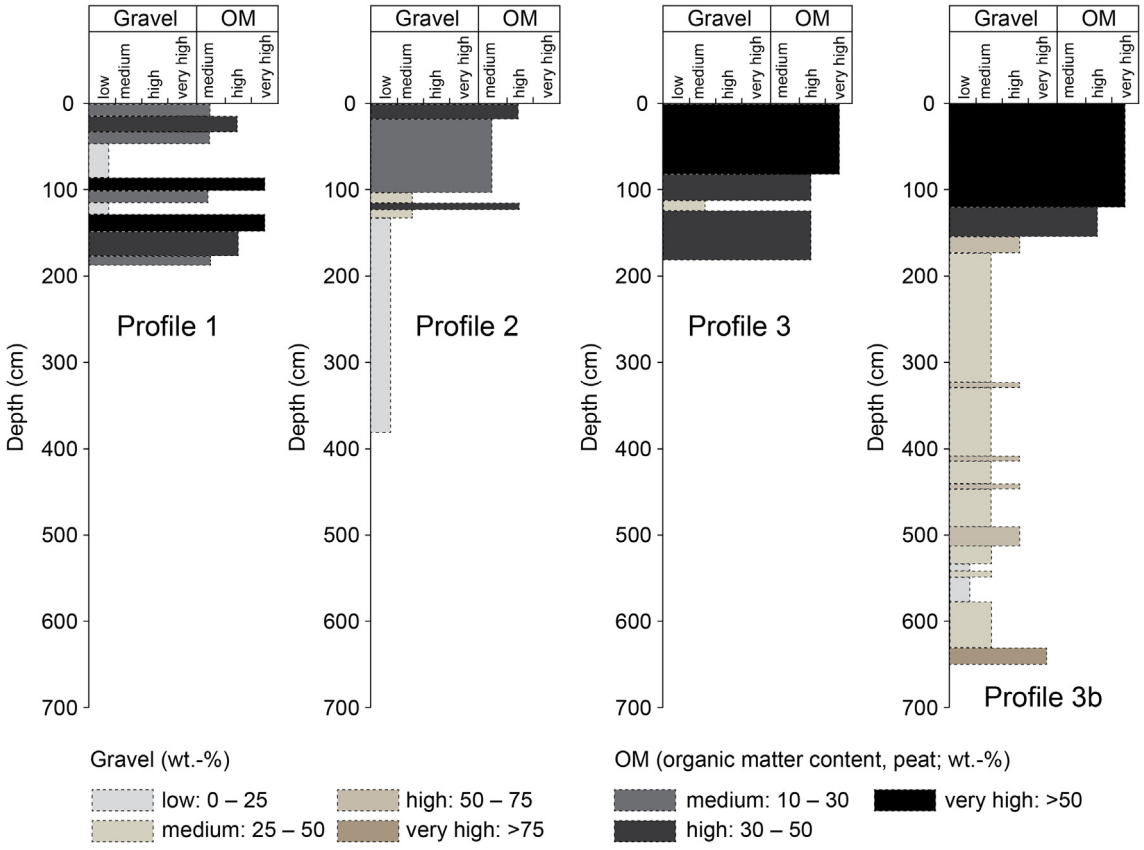

Fig. 5. Sediment logs of the mire profiles. The distinction of layers is primarily based on the organic matter (peat or decayed organic matter) and gravel content.

Pleistocene glacial maxima previously recorded from the WRR (Phillips et al., 1997; Dahms, 2004; Dahms et al., 2018). The array of moraine boulder surface ages reported here corresponds to these several glacial periods. We attribute the moraine adjacent to the mire to at least MIS16. Associated with the terminology used for the Wind River Range, this corresponds to the Sacagawea Ridge or possibly to a 'pre-Sacagawea Ridge' stage (Dahms, 2004; Dahms et al., 2018). The oldest exposure ages have a relatively large uncertainty. But even with the 1σ external uncertainty the ages are clearly above the next younger series of boulders (DIP-3, DIP-4 and DIP-5) that correlate well with the Bull lake stage (MIS 6; Dahms et al., 2018). DIP-3 and DIP-4 seem younger than DIP-5 but when considering the error range of the ages, they belong to the same unit. The age of boulder DIP-6 suggests the presence of a separate lateral moraine deposited by an ice advance here during MIS4. Although no numeric ages have been reported until now, relative age-data from moraines in similar positions (between MIS6 and MIS2) are reported from several nearby localities (Colman and Pierce, 1986; Hall and Shroba, 1995; Dahms, 2004) as well as from Asia (Finkel

Table 4
Radiocarbon data of the sampled profiles.

	uzh-sample code	Depth (cm)	Material	C14 age BP	±1σ	F14C	±1σ	δ13C ‰	±1σ	cal BP 2σ-range
Profile 1	6471	10–20	Peat	90	25	0.9888	0.0031	−37.1	1	260–25
	6472	90–100	Peat	2478	26	0.7346	0.0024	−29.9	1	2720–2437
	6473	130–140	Peat	2509	26	0.7318	0.0024	−30.3	1	2738–2490
Profile 2 + 2b	6475	23–35	Peat	273	25	0.9666	0.003	−27.4	1	430–155
	6476	102–115	Peat	3418	28	0.6535	0.0023	−27.6	1	3819–3584
	6499	110–120	Organic matter remain	2773[a]	23	0.7081	0.0020	−26.3	1	2994–2792
	6477	125–144	Peat	3776	29	0.625	0.0022	−26.2	1	4241–4010
	6501	350–360	Organic matter remain	4311	25	0.5847	0.0018	−24.5	1	4960–4836
Profile 3	6478	13–25	Peat	753	26	0.9105	0.0029	−28.5	1	727–666
	6513	45–57	Organic matter remain	6211	27	0.4616	0.0016	−23.9	1	7241–7009
	6514	76–89	Organic matter remain	9018[a]	31	0.3254	0.0013	−29.8	1	10,237–10,175
	6479	89–104	Peat	8553	38	0.3448	0.0016	−27.1	1	9555–9482
	6480	174–184	Peat	8944	39	0.3284	0.0016	−27.3	1	10,210–9917
Profile 3b	6502	20–50	Organic matter remain	223	22	0.9726	0.0026	−27.5	1	307–0
	6503	130–150	Organic matter remain	5243[b]	27	0.5206	0.0017	−28.8	1	6175–5923
	6504	220–230	Organic matter remain	5150[b]	26	0.5267	0.0017	−32.5	1	5987–5766
	6511	320–330	Organic matter remain	4992[b]	27	0.5372	0.0018	−32.4	1	5880–5650
	6512	340–350	Organic matter	6834	28	0.4271	0.0015	−31.5	1	7716–7608
	6507	460–470	Organic matter	9049	32	0.3242	0.0013	−30.3	1	10,245–10,188

[a] Considered as an outlier (for depth trend calculations).
[b] For linear age-depth modelling average value considered (age, depth).

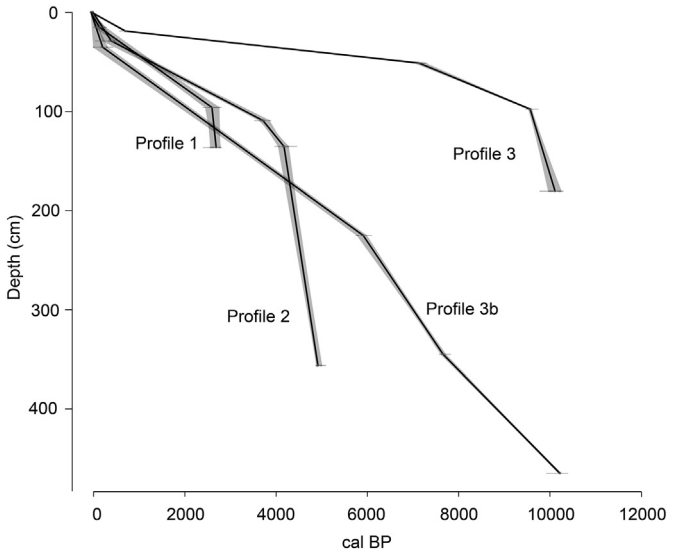

Fig. 6. Age-depth model the investigated cores using 'clam' (Blaauw, 2010).

et al., 2003; Ganyushkin et al., 2018). However, it is possible that this boulder simply may be toppled on the Bull lake moraine. The height of this boulder was about 2.5 m. With soil erosion (Section 4.2), it is possible that this boulder has changed its position over time. The surface ages of boulders DIP-7 and DIP-8 represent the LGM here as they overlap with the ages previously reported from LGM moraines in nearby Sinks and North Fork canyons (Dahms et al., 2018). The deepest sediment deposits of the Dickinson Park mire are, thus, probably much older than those we report here (about 10–11 ka). Given the geometry of the moraines, one would expect this mire to be active for much longer. However, no organic material was found at depths greater than we report here as drilling depth was limited by machine and manpower by the coarse sediments below ~7 m.

5.2. Mire and sediments

5.2.1. Early Holocene (11.5–7 kyr BP)

During the Holocene, geomorphic responses to several cold and warm phases have contributed to the formation of both local and regional landscapes (Booth et al., 2005). The transition from Late Pleistocene environmental conditions to those of the Holocene is characterised by distinct phases of erosion and sedimentation. In some montane regions, erosion rates increased by a factor of 5–10 when compared to LGM or pre-LGM times (Raab et al., 2019). This seems also to be the case in our study area; sedimentation rates and, thus, geomorphic slope erosion processes distinctly increased during this time. In the early Holocene of Europe, several rapid climate changes are reported around 11.1, 10.3, 9.4 and 8.2 ka BP (Florescu et al., 2019). Similarly, Hou et al. (2011) report abrupt cooling events in North America centered on 10.6, 10.2, 9.5, 9.2, 8.8 and 8.4 ka BP.

Some minor chemical changes occur in our mire profiles during these periods (9.4 and 10.3 ka BP), but the temporal resolution of the sedimentation rates (in mm yr^{-1}) remains inconclusive. If we consider the total mass deposited per unit area (t km^{-2} yr^{-1}), we see a small sedimentation peak near 9.4 ka BP (Fig. 11). Krause and Whitlock (2013) describe a step-like transition to higher summer temperatures at 11.5 ka BP in the Yellowstone region. They attribute increasing temperatures to be the primary control of vegetation change here. However, increased fire activity apparently facilitated and preceded the development of a closed forest (Krause and Whitlock, 2013).

It also appears that a phase of rapid and intense soil erosion (regressive soil evolution) is related to rapid climate deterioration that occurred at about 8.4 ka calBP. This event is recorded in several archives worldwide (Savi et al., 2014; Malkiewicz et al., 2016; Boxleitner et al., 2017). This phase is characterised in most reports by strong erosional processes leading to regressive soil evolution. One distinct arid event is recorded in the sediments of Emerald Lake (Colorado) at 8200 calBP (Jimnénez-Moreno et al., 2019) and is characterised by evidence of a low lake level along with a prominent vegetation change. Overall, this region of the Rocky Mountains became cooler and drier and even more windy (Alley et al., 1997; Berger and Guilaine, 2009). We cannot, however, clearly identify this event in Dickinson Park through geochemical traces nor increased sedimentation rates. Rather, our findings fit more closely to those of Shuman (2012) who detected no temperature anomalies in nearby Yellowstone National Park (about 200 km to the northwest) and the Bighorn Mountains (about 230 km to the northwest). Maxbauer et al. (2020) suggest a hydroclimatic response to the 8.2 ka event in the Northern Rockies that is not previously documented, based on magnetic properties of lake sediments. They suggest that arid conditions prevailed in this region until more humid conditions returned at about 3 ka BP. Lu et al. (2017) show that the Yellowstone-region lake ecosystems underwent shifts in the diatom community structure at 11.3–11.0 and 8.8–8.7 ka BP. They infer that large-scale climatic change was the principal driver of ecosystem evolution. They assumed that increasing moisture caused the changes in diatoms at about 8.8 ka BP. If we consider that the sedimentation and erosion rates in the Dickinson Park mire only slightly increased at the transition to the Holocene (Fig. 11) and that the deposited material was rather weakly weathered (Figs. 8–10), particularly at about 8–9 kyr BP, then this suggests that this area exhibited rather low chemical weathering conditions in response to a relatively dry but cool climate. This assumption is supported by findings of Krause and Whitlock (2013) who showed that climatic conditions in northern Yellowstone became cooler and drier at about 8.2 ka BP.

The general climatic trends between about 11.7 and 7.0 ka BP are moderately comparable among localities in Alaska, British Colombia, central/southern Cascades, Sierra Nevada, northern Rocky Mountains and southern Rocky Mountains (Palacios et al., 2020). The glacier extents in these regions was about 0–20% compared to the global Last Glacial Maximum. This, however, does not exclude the existence of local-to-regional temporal differences as comparatively cooler and wetter conditions seem to have persisted during this period in Mexico and Northern Andes (Palacios et al., 2020).

5.2.2. Middle Holocene (7–4 kyr BP)

Shuman (2012) and Shuman and Marsicek (2016) reconstructed maximum Holocene temperatures for the period around 6800 calBP. After this period, about 5.9 ka, another rapid climate change is reported by Florescu et al. (2019) who note that this event (like several others) is often not clearly reflected in continental archives. It seems that, during the period of note, erosion and sedimentation rates were slightly higher than usual; but how they are related to the 5.9 ka event remains uncertain.

In several parts of the world, a distinct cold event is detected around 4.2 ka BP (Magny, 2004; Berger and Guilaine, 2009; Engel et al., 2010; Brisset et al., 2013). Booth et al. (2005) and Florescu et al. (2019) also identified this abrupt cool-climate pulse and/or rapid environmental changes in other regions of the Northern Hemisphere. In some regions this climatic shift has been overprinted by human impacts on landscapes. This climatic shift seems to have been accompanied by higher erosion and accumulation rates (Boxleitner et al., 2017) in remote subboreal and alpine areas. Jimnénez-Moreno et al. (2019) showed that a combination of insolation changes occurred at this time, accompanied by a significant cold/arid event and a change in precipitation patterns associated with weakening of the North American Monsoon (NAM) and stronger winter precipitation dynamics. We detect a clear signal of this period in the Dickinson Park mire (Fig. 11). The changes in chemical parameters and sedimentation rates in the mire appear to

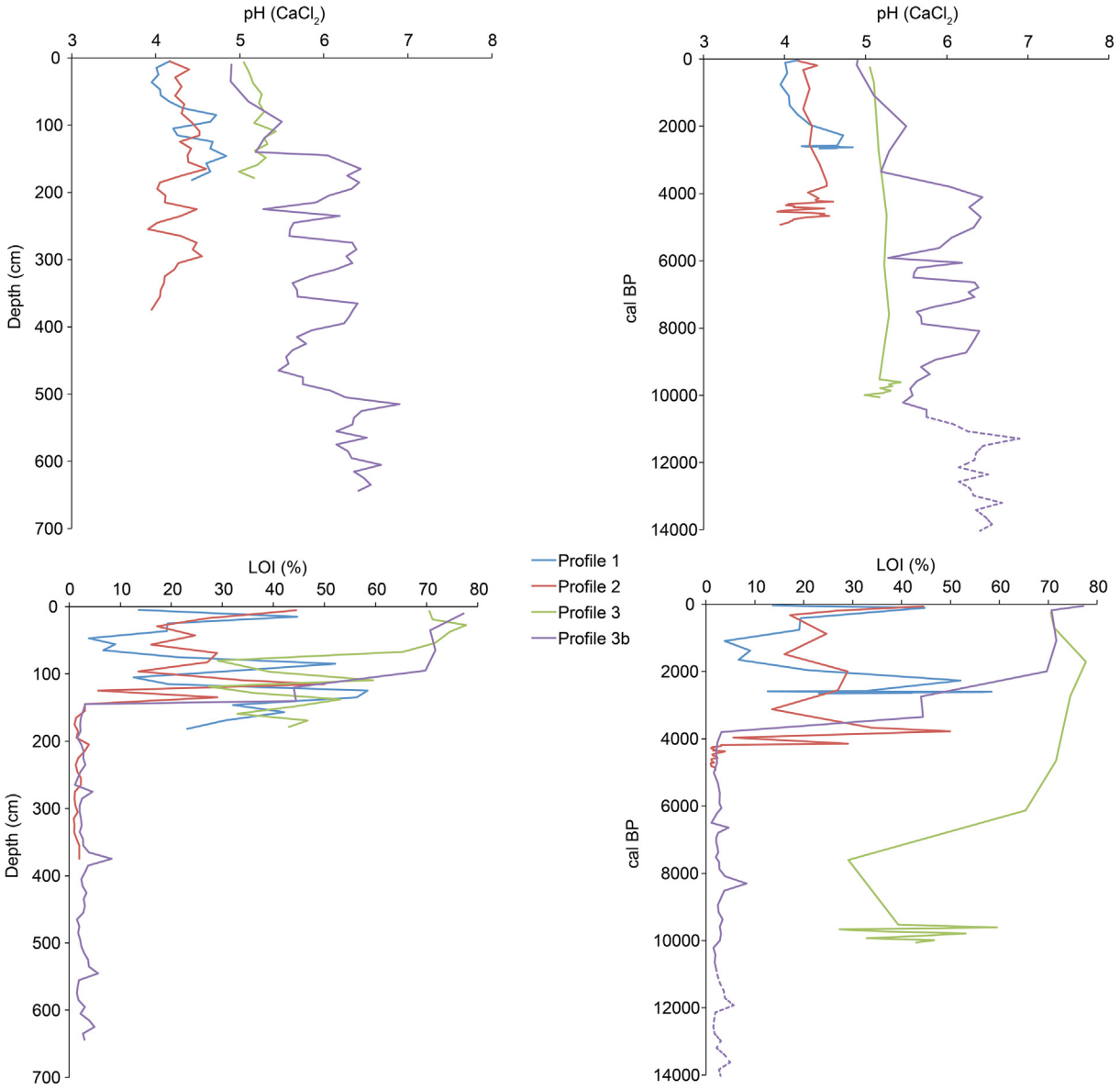

Fig. 7. pH-value and LOI as a function of core depth (mire) and extrapolated time.

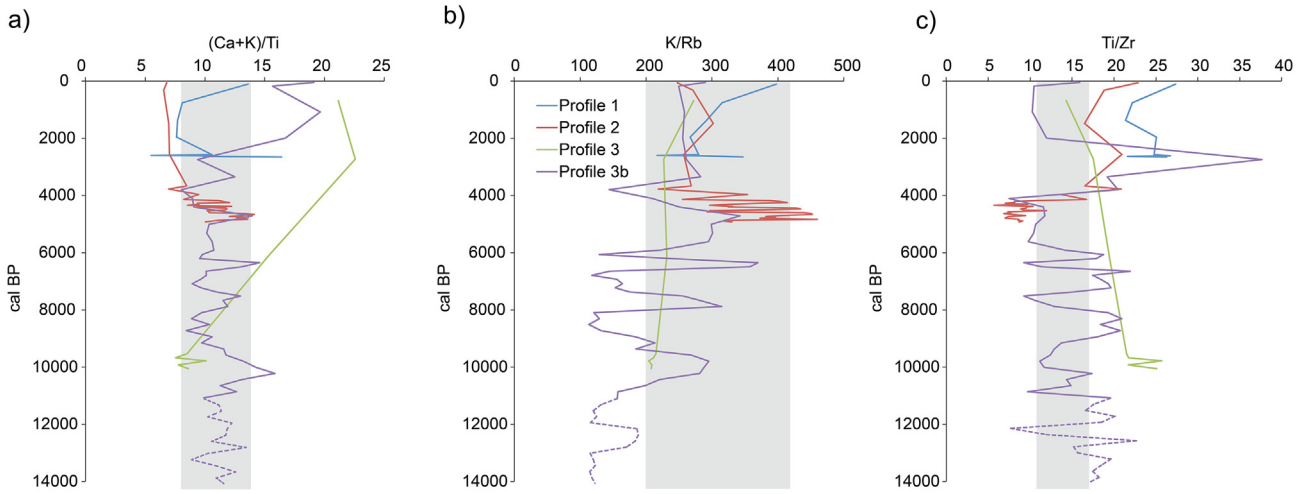

Fig. 8. a) Weathering (Ca + K)/Ti, b) K/Rb and c) Ti/Zr ratio of the mire cores and as a function of time. The grey area indicates the measured range in the adjacent soils (DP1–5).

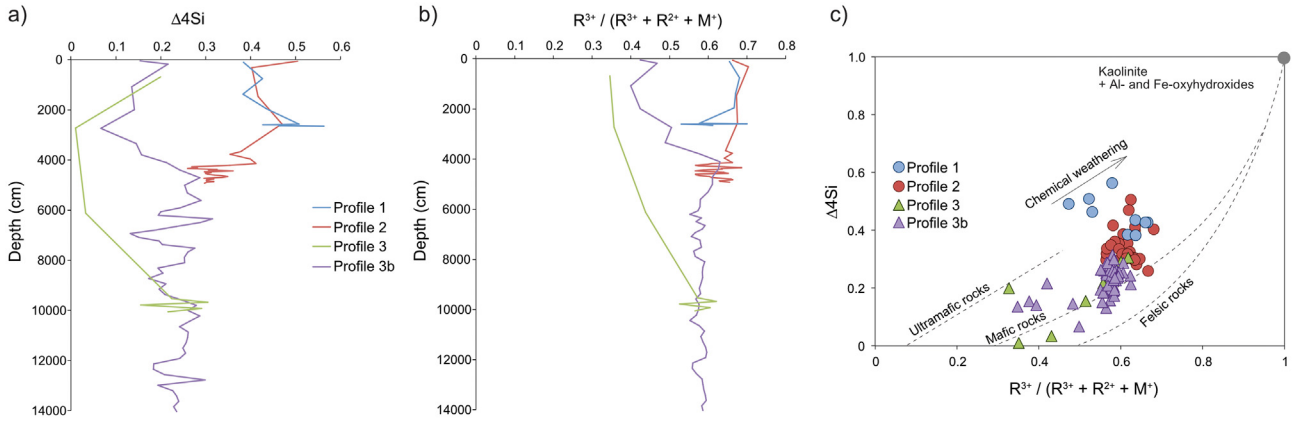

Fig. 9. a) Difference to the maximum alteration to kaolinite (Δ4Si) and b) ratio of trivalent cations as a function of time (mire cores); c) weathering reaction trend towards kaolinite, based on Δ4Si and ratio to trivalent cations (according to Meunier et al., 2013 and Fang et al., 2019).

coincide with the cold phases as presented in Boxleitner et al. (2017) and Jimnénez-Moreno et al. (2019). The higher sedimentation rates, the partially lower (Ca + K)/Ti ratio (Fig. 11), the strongly increasing formation of Al(o) (Fig. 10) may be indicative of wetter conditions. This would partially contradict the results of Maxbauer et al. (2020). It moderately well fits to the paleoecological records in the northern Rocky Mountains that indicate prolonged warm dry conditions as late as 3500 cal BP (Krause and Whitlock, 2013). This suggests that, due to climatic and non-climatic feedbacks, the transition to middle Holocene conditions did not occur synchronously throughout the region.

Considerations of the $R^{3+}/(R^{3+} + R^{2+} + M^{+})$ ratios, the Fe (o) contents, pH values or (Ca + K)/Ti ratios (Figs. 8–10) show that weathering conditions in this area of the WRR seems to have been moderate-to-weak before about 5–6 ka BP. More intense chemical weathering and soil formation seem to have been the case since then. This trend, however, is not reflected in all our cores. Nonetheless, our results suggest that chemical weathering began to increase after the mid-Holocene aridity period (from 8 to 5.5 ka BP; Shuman and Serravezza, 2017). This is consistent with the reported rapid increase in effective moisture across much of western North America from 6 to 4 ka (Shuman and Serravezza, 2017).

5.2.3. Late Holocene (4–0 kyr BP)

Cold phases are reported from the Swiss Alps around 3–2.3 ka BP and 1.8–1.1 ka BP as the 'Göschenen cold phases' (see Boxleitner et al., 2019). However, Boxleitner et al. questions the glaciological definition of the Göschenen Cold Phases as 'glacier advances', showing that these phases are not suitable as reference stadials in the system of Alpine Holocene glacier fluctuations. These findings, however, do not mean that cold phases did not occur during these periods. In Dickinson Park, one profile shows a distinct increase in sedimentation rate beginning about 4 ka BP (Fig. 11). In nearby regions of Wyoming and Colorado, Whitlock et al. (2011) and Jimnénez-Moreno et al. (2019) report drier conditions at this time together with associated changes in vegetation. An additional cool phase associated with increased erosion and sedimentation (Fig. 11) was the Little Ice Age (LIA). From the 15th to the 19th century, the well-documented LIA accelerated many geomorphic surface processes.

Significant organic matter accumulation began around 10 ka BP at Dickinson Park Core #3, whereas at the other core sites, this process apparently began only around 4 ka. The high sedimentation rates identified in cores 1,2 and 3b, as expressed in mm yr^{-1}, apparently reflect the accumulation of organic matter more than the sediment influx

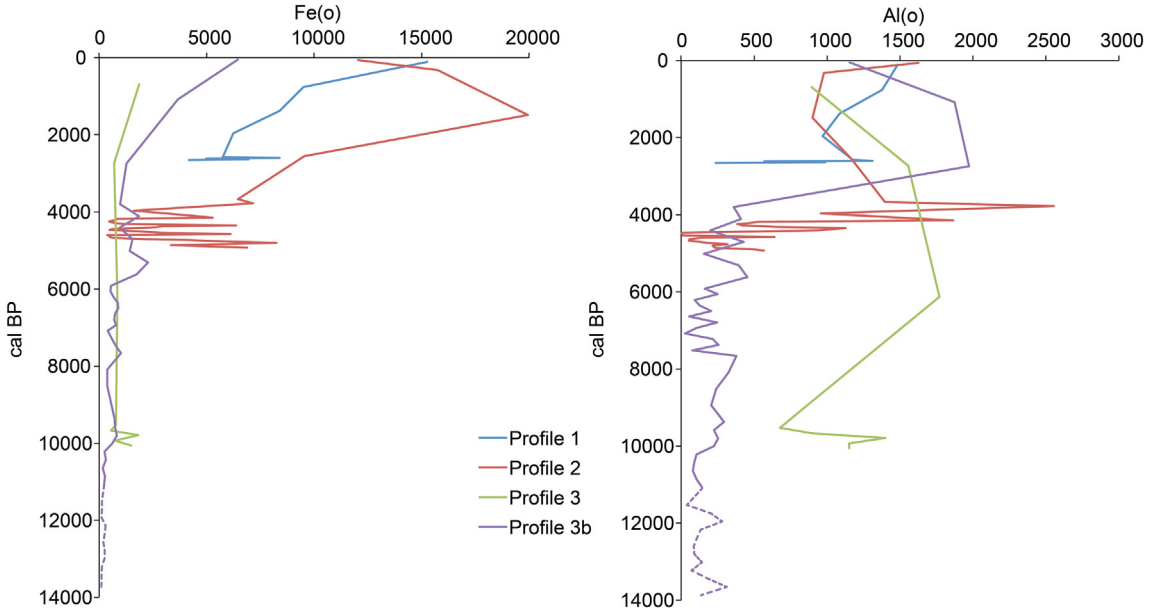

Fig. 10. Oxalate extractable Fe and Al along the mire cores and as a function of time.

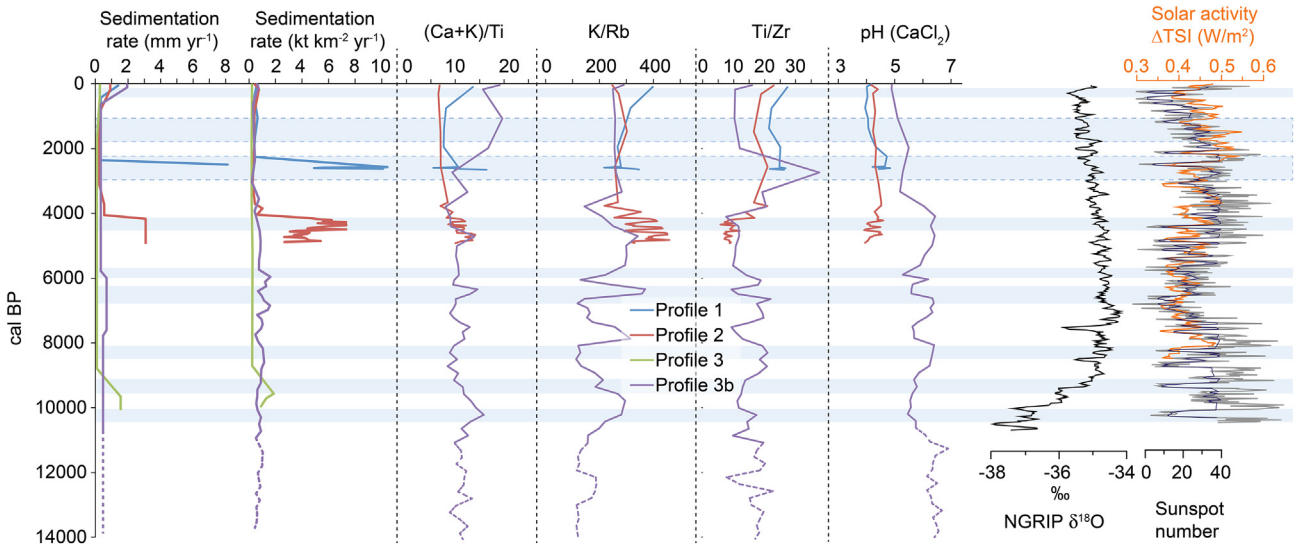

Fig. 11. Visual correlation of some selected parameters (sedimentation rate, weathering index (Ca + K)/Ti, K/Rb- and Ti/Zr-ratio and pH-value) with changing climatic indicators over time. Due to the relatively low temporal resolution, profile 3 was not considered for the geochemical parameters (cf. Figs. 5 and 6). The compilation of solar activity data, sunspot number and NGRIP $\delta^{18}O$ are from Florescu et al. (2019).

into the mire. Thus, with respect to the mass of material deposited in these areas of the mire (t km^{-2} yr^{-1}), the actual sedimentation rates did not increase.

The mire and its surrounding area apparently did not, in aggregate, show a uniform reaction to changing climatic conditions. Nonetheless, although different core locations responded in differing ways, we can detect a general soil redistribution pattern here. We find that deposition rates (and thus erosion rates of the adjacent soils and surfaces) were higher during almost all known Holocene cool phases. In some cases (particularly in profile 3), the deposited material was less weathered. Profile 3b seems to be driven more by stream activity and the subsequent input of less weathered material (shallow landslides?), whereas sites 1 and 2 clearly are influenced by erosion of the soils on the adjacent slopes. The K/Rb ratio at site 3b and particularly the Ti/Zr ratio at sites 1,2 and 3b sometimes are clearly outside the range measured in the soils. The higher ratios of Ti/Zr and lower values of K/Rb may indicate allochthonous sources such as dust input. According to the published and unpublished data of Dahms et al. (2012), the Ti/Zr ratios in soils of the adjacent Middle Popo Agie basin (Sinks Canyon up to Stough Creek Basin and Big Foot Lake) varies from 9 to 29. The highest values were measured in the alpine localities in Stough Creek Basin. It seems therefore likely that aeolian material is admixed into the deposits at Dickinson Park. This aeolian input became more evident during the last about 2500 years. Its origin could be mostly local but the aeolian influx patterns previously reported from the WRR and elsewhere in the region strongly suggests the presence of a regional pattern of dust accumulation in alpine areas of the western U.S. (Colman and Pierce, 1986; Dahms, 1993, 2002; Dahms and Rawlins, 1996; Applegarth and Dahms, 2004; Portes et al., 2018; Munroe et al., 2015; Munroe et al., 2020). In particular, the prairies of the Midwestern states became continuously warmer (and drier) over the last 2000 years (Viau et al., 2012). This trend triggers an increased aeolian transport.

Most of the reported Holocene climatic perturbations of 10.2, 9.4, 8.2, 5.9 and 4.2 ka BP were generally events identified as cold and/or arid (Florescu et al., 2019; Jimnénez-Moreno et al., 2019). However, strongly regional differences exist, and in several cases, the evidence for aridity or humidity are ambivalent. The events at about 2.9 and 1.4 ka apparently were less dry. Our data shows that geomorphic activity (erosion/deposition) particularly increased during the cold events at 10.2 to 9.4 ka BP, 4.2 and about 2.4 ka BP.

6. Conclusion

Based on our five mire core profiles, we find that it is generally possible to reconstruct those geomorphic processes (net deposition/erosion) active in the region surrounding this locality for the last ca. 11 ka. The moraine complex adjacent to the mire is composed of lateral moraines emplaced during several advances of the North Fork valley glacier from at least MIS16 up to MIS2. As a consequence, older sediments are probably present in the mire, but were inaccessible to us. Using this geoforensic approach, we identify signals of increased geomorphic activity that match known cold (and often dry) events of the Holocene. However, an increase in purported geomorphic activity was not detected in each profile (assuming that surface processes often were spatially dispersed). A higher deposition rate (and consequently associated erosion of adjacent soils) was observed for the known cold periods 9.4–10.2 ka BP, 4.2 ka BP, 2.5 ka BP and during the LIA, but the mass deposition rates were not higher during the LIA, due to the continual aggradation of organic matter and, thus, the formation of the mire. The results from this mire support the concept of relatively cool but probably rather dry climate conditions during the early Holocene in the transition region of the northern to the southern Rocky Mountains. However, this remains still slightly speculative as inconsistent results exist in the literature. Surprisingly, no particular changes in rates of deposition are detected that correspond to the 8.2 ka cold event that, in general, still is not well documented in the Rocky Mountains. Although mostly drier conditions are reported to prevail during these cold events, enough water appears to have been available here to allow an increase in geomorphic activity. We detect increased weathering intensity and soil formation for roughly the last 5 kyr that is apparently due to a general increase in available moisture. This seems partly to contradict the findings of other workers who hypothesised that the Northern Rocky Mountains had a rather dry climate until about 3 ka BP. During the same period (last 5 kyr), more organic matter accumulated and aeolian deposition became more evident in our Dickinson Park cores. Our investigation also generally shows that this landscape reacted in a rather "patchy" manner; that is, that only selected archives may indicate environmental deterioration during changes towards cool/dry episodes. We

furthermore show, that the selection of just 1 single profile per lake or mire might not be enough to detect all environmental changes. Sediment input into lakes or mires may vary spatially (as they evidently do here), so that events may be missed or detected by chance.

Supplementary data to this article can be found online at https://doi.org/10.1016/j.geomorph.2020.107433.

Declaration of competing interest

The authors declare that they have no known competing financial interests or personal relationships that could have appeared to influence the work reported in this paper.

Acknowledgements

We thank Tatjana Kraut and Thomy Keller for their support in the laboratory. We are indebted to two unknown reviewers and Matteo Spagnolo for their helpful and constructive comments on an earlier version of the manuscript. We also thank the Eastern Shoshone Nation of the Wind River Reservation for access to the Dickinson Park locality, and to the Diamond 4 Ranch for their hospitality during our fieldwork.

References

Alley, R.B., Vlark, P.U., 1999. The deglaciation of the northern hemisphere: a global perspective. Annu. Rev. Earth Planet. Sci. 27, 149–182. https://doi.org/10.1146/annurev.earth.27.1.149.

Alley, R.B., Mayewski, P.A., Sowers, T., Stuiver, M., Tayler, K.C., Clark, P.U., 1997. Holocene climatic instability: a prominent, widespread event 8200 yr ago. Geology 25, 483–486.

Applegarth, M.T., Dahms, D., 2004. Aeolian modification of moraine soils, Whiskey Basin, Wyoming, USA. Earth Surf. Proc. Land. 29, 579–585. https://doi.org/10.1002/esp.1052.

Berger, J.F., Guilaine, J., 2009. The 8200 calBP abrupt environmental change and the Neolithic transition: a Mediterranean perspective. Quat. Int. 200, 31–49.

Blaauw, M., 2010. Methods and code for 'classical' age-modelling of radiocarbon sequences. Quat. Geochronol. 5, 512–518.

Booth, R.K., Jackson, S.T., Forman, S.L., Kutzbach, J.E., Bettis, I.E.A., Kreig, J., Wright, D.K., 2005. A severe centennial-scale drought in midcontinental North America 4200 years ago and apparent global linkages. The Holocene 15, 321–328.

Boxleitner, M., Musso, A., Waroszewski, J., Makiewicz, M., Maisch, M., Dahms, D., Brandová, D., Christl, M., de Castro Portes, R., Egli, M., 2017. Late Pleistocene – Holocene surface processes and landscape evolution in the central Swiss Alps. Geomorphology 295, 306–322.

Boxleitner, M., Ivy-Ochs, S., Brandová, D., Christl, M., Egli, M., Maisch, M., 2019. Lateglacial and Early Holocene glacier stages - New dating evidence from the Meiental in central Switzerland. Geomorphology 340, 15–31. https://doi.org/10.1016/j.geomorph.2019.04.004.

Bradley, S.R., Bakke, J., 2019. Is there evidence for a 4.2 ka BP event in the northern North Atlantic region? Clim. Past 15, 1665–1676. https://doi.org/10.5194/cp-15-1665-2019.

Brewer, J.A., Allmendinger, R.W., Brown, L.D., Oliver, J.E., Kaufman, S., 1982. COCORP profiling across the Rocky Mountain Front in southern Wyoming, part 1: Laramide Structure. Geol. Soc. Am. Bull. 93, 1242–1252.

Brisset, E., Miramont, C., Guiter, F., Anthony, E., Tachikawa, K., Poulenard, J., Arnaud, F., Delhon, F., Meunier, J.-D., Bard, E., Sumera, F., 2013. Non-reversible geosystem destabilisation at 4200 cal. BP: sedimentological, geochemical and botanical markers of soil erosion recorded in a Mediterranean alpine lake. The Holocene 23, 1863–1874. https://doi.org/10.1177/0959683613508158.

Chmeleff, J., von Blanckenburg, F., Kossert, K., Jakob, D., 2010. Determination of the ^{10}Be half-life by multicollector ICP-MS and liquid scintillation counting. Nucl. Instrum. Methods Phys. Res. Sect. B 268, 192–199.

Christl, M., Vockenhuber, P.W., Kubik, P.W., Wacker, L., Lachner, J., Alfimov, V., Synal, H.-A., 2013. The ETH Zurich AMS facilities: performance parameters and reference materials. Nucl. Inst. Methods Phys. Res. B 294, 29–38.

Colman, S.M., Pierce, K.L., 1986. Glacial sequence near McCall, Idaho: weathering rinds, soil development, morphology, and other relative age criteria. Quat. Res. 25, 25–42.

Condie, K.C., 1993. Chemical composition and evolution of the upper continental crust: contrasting results from surface samples and shales. Chem. Geol. 104, 1–37. https://doi.org/10.1016/0009-2541(93)90140-E.

Copeland, H.E., Tessman, S.A., Girvetz, E.H., Roberts, L., Enquist, C., Orabona, A., Patla, S., Kiesecker, J., 2010. A geospatial assessment on the distribution, condition, and vulnerability of Wyoming's wetlands. Ecol. Indic. 10, 869–879.

Dahms, D.E., 1993. Mineralogical evidence for eolian sediments in soils on late Quaternary moraines, Wind River Mountains, Wyoming. Geoderma 59, 175–196.

Dahms, D.E., 2002. Glacial stratigraphy of Stough Creek basin, Wind River Range, Wyoming. Geomorphology 42, 59–83.

Dahms, D.E., 2004. Relative and numeric age data for pleistocene glacial deposits and diamictons in and near Sinks Canyon, Wind River Range, Wyoming, U.S.A. Arct. Antarct. Alp. Res. 36, 59–77.

Dahms, D.E., Rawlins, C.L., 1996. A two-year record of eolian sedimentation in the Wind River Range, Wyoming, U.S.A. Arct. Alp. Res. 28, 210–216.

Dahms, D.E., Birkeland, P.W., Shroba, R.R., Miller, C., Dan, Kihl, R., 2010. Latest Quaternary Glacial and Periglacial Stratigraphy, Wind River Range, Wyoming. Geol. Soc. Am., Digital Maps and Charts Series 7 46. https://doi.org/10.1130/2010.DMCH007.

Dahms, D., Favilli, F., Krebs, R., Egli, M., 2012. Soil weathering and accumulation rates of oxalate-extractable phases from alpine chronosequences of up to 1 Ma in age. Geomorphology 151-152, 99–113.

Dahms, D., Egli, M., Fabel, D., Harbor, J., Brandová, D., Portes, R., Christl, M., 2018. Revised Quaternary glacial succession and post-LGM recession, southern Wind River Range, Wyoming, USA. Quat. Sci. Rev. 192, 167–184. https://doi.org/10.1016/j.quascirev.2018.05.020.

Egli, M., Mirabella, A., Fitze, P., 2001. Clay mineral formation in soils of two different chronosequences in the Swiss Alps. Geoderma 104, 145–175.

Engel, Z., Nývlt, D., Křížek, M., Treml, V., Jankovská, V., Lisá, L., 2010. Sedimentary evidence of landscape and climate history since the end of MIS 3 in the Krkonoše Mountains, Czech Republic. Quat. Sci. Rev. 29, 913–927.

Fang, Q., Hong, H., Algeo, T.J., Huang, X., Sun, A., Churchman, G.J., Chorover, J., Chen, S., Liu, Y., 2019. Microtopography-mediated hydrologic environment controls elemental migration and mineral weathering in subalpine surface soils of subtropical monsoonal China. Geoderma 344, 82–98. https://doi.org/10.1016/j.geoderma.2019.03.008.

Finkel, R.C., Owen, L.A., Barnard, P.L., Caffee, M.W., 2003. Beryllium-10 dating of Mount Everest moraines indicates a strong monsoon influence and glacial synchroneity throughout the Himalaya. Geology 31, 561–564.

Florescu, G., Brown, K.J., Carter, V.A., Kuneš, P., Veski, S., Feurdean, A., 2019. Holocene rapid climate changes and ice-rafting debris events reflected in high-resolution European charcoal records. Quat. Sci. Rev. 222, 105877. https://doi.org/10.1016/j.quascirev.2019.105877.

Frost, B.R., Frost, C.D., Hulsebosch, T.P., Swapp, S.M., 2000. Origin of the charnockites of the Louis Lake batholith, Wind River Range. Wyoming. J. Petrol. 41, 1759–1776.

Ganyushkin, D., Chistyakov, K., Volkov, I., Bantcev, D., Kunaeva, E., Brandová, D., Raab, G., Christl, M., Egli, M., 2018. Palaeoclimate, glacier and treeline reconstruction based on geomorphic evidences in the Mongun-Taiga massif (south-eastern Russian Altai) during the Late Pleistocene and Holocene. Quat. Int. https://doi.org/10.1016/j.quaint.2017.12.031.

Gosse, J.C., Phillips, F.M., 2001. Terrestrial in situ cosmogenic nuclides: theory and application. Quat. Sci. Rev. 20, 1475–1560.

Hall, R.D., Shroba, R.R., 1995. Soil evidence for a glaciation intermediate between the Bull Lake and Pinedale glaciations at Fremont Lake, Wind River Range, Wyoming, USA. Arct. Alp. Res. 27, 89–98.

Harrington, C.D., Whitney, J.W., 1987. Scanning electron microscope method of rock-varnish dating. Geology 15, 967–970.

Harris, S.A., 2019. The relationship of sea level changes to climatic change in northeast Asia and northern North America during the last 75 ka B.P. AIMS Environ. Sci. 6 (1), 14–40. https://doi.org/10.3934/environsci.2019.1.14.

Harrison, S., Mighall, T., Stainforth, D.A., Allen, P., Macklin, M., Anderson, E., Knight, J., Mauquoy, D., Passmore, D., Rea, D., Spagnolo, M., Shannon, S., 2019. Uncertainty in geomorphological responses to climate change. Climate Change 156, 69–86. https://doi.org/10.1007/s10584-019-02520-8.

Heidel, B., 2013. Sensitive Plant Survey in the Dickinson Park Area. Prepared for the Shoshone National Forest. Wyoming Natural Diversity Database, Laramie, WY.

Hou, J., Huang, Y., Shuman, B.N., Oswald, W.V., Foster, D.R., 2011. Abrupt cooling repeatedly punctuated early-Holocene climate in eastern North America. The Holocene 22, 525–529. https://doi.org/10.1177/0959683611427329.

Jimnénez-Moreno, G., Anderson, R.S., Shuman, B.N., Yackulic, E., 2019. Forest and lake dynamics in response to temperature, North American monsoon and ENSO variability during the Holocene in Colorado (USA). Quat. Sci. Rev. 211, 59–72. https://doi.org/10.1016/j.quascirev.2019.03.013.

Kabara-Pendias, A., Pendias, H., 2000. Trace Elements in Soils and Plants (Third Edition).

Krause, T.R., Whitlock, C., 2013. Climate and vegetation change during the late-glacial/early-Holocene transition inferred from multiple proxy records from Blacktail Pond, Yellowstone National Park, USA. Quat. Res. 79, 391–402. https://doi.org/10.1016/j.yqres.2013.01.005.

Krause, T.R., Lu, Y., Whitlock, C., Fritz, S.C., Pierce, K.L., 2015. Patterns of terrestrial and limnologic development in the northern Greater Yellowstone Ecosystem (USA) during the late-glacial/early-Holocene transition. Palaeogeography, Palaeoclimatology, Palaeoecology 422, 46–56. https://doi.org/10.1016/j.palaeo.2014.12.018.

Lal, D., 1991. Cosmic ray labeling of erosion surfaces: in situ nuclide production rates and erosion models. Earth Planet. Sci. Lett. 104, 424–439.

Lamentowitcz, M., Galka, M., Lamentowitcz, L., Obremnska, M., Kühl, N., Lücke, A., Jassey, V.E.J., 2015. Reconstructing climate change and ombrotrophic bog development during the last 4000 years in northern Poland using biotic proxies, stable isotopes and trait-based approach. Palaeogeography, Palaeoclimatology. Palaeoecology 418, 261–277.

Love, J.D., Christianson, A.C., 1985. Geologic Map of Wyoming. U. S. Geological Survey. Map scale 1: 500,000.

Lu, Y., Stone, J., Fritz, S.C., Westover, K., 2017. Major climatic influences on Yellowstone-region lake ecosystems suggested by synchronous transitions in Late-Glacial and early-Holocene diatom assemblages. Palaeogeogr. Palaeoclimatol. Palaeoecol. 485, 178–188. https://doi.org/10.1016/j.palaeo.2017.06.011.

Magny, M., 2004. Holocene climate variability as reflected by mid-European lake-level fluctuations and its probable impact on prehistoric human settlements. Quat. Int. 113, 65–79.

Malkiewicz, M., Waroszewski, J., Bojko, O., Egli, M., Kabala, C., 2016. Holocene vegetation history and soil development reflected in the lake sediments of the Karkonosze Mountains (Poland). The Holocene 26, 890–905.
Masarik, L., Wieler, R., 2003. Production rates of cosmogenic nuclides in boulders. Earth Planet. Sci. Lett. 216, 201e208.
Matero, I.S.O., Gregoire, L.J., Ivanvic, R.F., Tindall, J.C., Haywood, A.M., 2017. The 8.2 ka cooling event caused by Laurentide ice saddle collapse. Earth Planet. Sci. Lett. 473, 205–214. https://doi.org/10.1016/j.epsl.2017.06.011.
Maxbauer, D.P., Shapley, M.D., Geiss, C.E., Ito, E., 2020. Holocene climate recorded by magnetic properties of lake sediments in the Northern Rocky Mountains, USA. The Holocene 30, 479–484. https://doi.org/10.1177/09596836198874.
McKeague, J.A., Brydon, J.E., Miles, N.M., 1971. Differentiation of forms of extractable iron and aluminium in soils. Soil Sci. Soc. Am. Proc. 35, 33–38.
Meunier, A., Caner, L., Hubert, F., El Albani, A., Prêt, D., 2013. The weathering intensity scale (WIS): an alternative approach of the chemical index of alteration (CIA). Am. J. Sci. 313, 113–143. https://doi.org/10.2475/02.2013.03.
Mizota, C., van Reeuwijk, L.P., 1989. Clay mineralogy and chemistry of soils formed in volcanic material in diverse climate regions. International Soil Reference and Information Centre, Soil Monograph. vol. 2 Wageningen.
Moore, D.M., Reynolds, R.C., 1997. X-ray Diffraction and the Identification and Analysis of Clay Minerals. 2nd edition. Oxford University Press, New York.
Munroe, Jeffrey S., Attwood, Emily C., O'Keefe, Samuel S., Quackenbush, Paul J.M., 2015. Eolian deposition in the alpine zone of the Uinta Mountains, Utah, USA. Catena 124, 119–129.
Munroe, Jeffrey S., Norris, Emmet D., Olson, Pratt M., Ryan, Peter C., Tappa, Michael J., Beard, Brian L., 2020. Quantifying the contribution of dust to alpine soils in the periglacial zone of the Uinta Mountains, Utah, USA. Geoderma 378, 114631. https://doi.org/10.1016/j.geoderma.2020.114631.
Nishiizumi, K., Imamura, M., Caffee, M.W., Southon, J.R., Finkel, R.C., McAninch, J., 2007. Absolute calibration of 10Be AMS standards. Nucl. Instrum. Methods Phys. Res. Sect. B 258, 403–413.
Osborn, G., Menounous, B., Ryane, C., Riedel, J., Clague, J.J., Koch, J., Clark, D., Scott, K., Davis, P.T., 2012. Latest Pleistocene and Holocene glacier fluctuations on Mount Baker, Washington. Quat. Sci. Rev. 49, 33–51. https://doi.org/10.1016/j.quascirev.2012.06.004.
Palacios, D., Stokes, C.R., Phillips, F.M., Clague, J.J., Alcalá-Reygosa, J., Andrés, N., Angel, I., Blard, P.-H., Briner, J.P., Hall, B.L., Dahms, D., Hein, A.S., Jomelli, V., Mark, B.G., Martini, M.A., Moreno, P., Riedel, J., Sagredo, E., Stansell, N.D., Vázquez-Selem, L., Vuille, M., Ward, D.J., 2020. The deglaciation of the Americas during the last glacial termination. Earth Sci. Rev. 103113. https://doi.org/10.1016/j.earscirev.2020.103113.
Phillips, F.M., Zreda, M.G., Gosse, J.C., Klein, J., Evenson, E.B., Hall, R.D., Chadwick, O.A., Sharma, P., 1997. Cosmogenic 36Cl and 10Be ages of Quaternary glacial and fluvial deposits of the Wind River Range. Wyoming. Geol. Soc. Am. Bull. 109, 1453e1463.
Portes, R., Dahms, D., Brandová, D., Raab, G., Christl, M., Kühn, P., Ketterer, M., Egli, M., 2018. Evolution of soil erosion rates in alpine soils of the Central Rocky Mountains using fallout Pu and $\delta^{13}C$. Earth Planet. Sci. Lett. 496, 257–269. https://doi.org/10.1016/j.epsl.2018.06.002.
Raab, G., Egli, M., Norton, K., Dahms, D., Brandová, D., Christl, M., Scarciglia, F., 2019. Climate and relief-induced controls on the temporal variability of denudation rates in a granitic upland. Earth Surf. Process. Landf. 44, 2570–2586. https://doi.org/10.1002/esp.4681.
Ran, M., Chen, L., 2019. The 4.2 ka BP climatic event and its cultural responses. Quat. Int. 521, 158–167. https://doi.org/10.1016/j.quaint.2019.05.030.
Reimer, P.J., Bard, E., Bayliss, A., Beck, J.W., Blackwell, P.G., Bronk Ramsey, C., Buck, C.E., Cheng, H., Edwards, R.L., Friedrich, M., Grootes, P.M., Guilderson, T.P., Haflidason, H., Hajdas, I., Hatté, C., Heaton, T.J., Hoffmann, D.L., Hogg, A.G., Hughen, K.A., Kaiser, K.F., Kromer, B., Manning, S.W., Nui, M., Reimer, R.W., Richards, D.A., Scott, E.M., Southon, J.R., Staff, A.R.A., Turney, C., van der Plicht, J., 2013. IntCal13 and Marine13 radiocarbon age calibration curves 0–50,000 years cal BP. Radiocarbon 55, 1869–1887.
Savi, S., Norton, K., Picotti, V., Akçar, N., Delunel, R., Brardinoni, F., Kubik, P., Schlunegger, F., 2014. Quantifying sediment supply at the end of the last glaciation: dynamic reconstruction of an alpine debris-flow fan. GSA Bull. 126, 773–790.
Shakun, J.D., Carlson, A.E., 2010. A global perspective on Last Glacial Maximum to Holocene climate change. Quat. Sci. Rev. 29, 1801e1816.
Shuman, B., 2012. Recent Wyoming temperature trends, their drivers, and impacts in a 14,000-year context. Clim. Change 112 (2), 429–447.
Shuman, B.N., Marsicek, J., 2016. The structure of Holocene climate change in midlatitude North America. Quat. Sci. Rev. 141, 38e51.
Shuman, B.N., Serravezza, M., 2017. Patterns of hydroclimatic change in the Rocky Mountains and surrounding regions since the last glacial maximum. Quat. Sci. Rev. 173, 58–77.
Silva-Sánchez, N., Schofield, J.E., Mighall, T.M., Cortizas, A.M., Edwards, K.J., Foster, I., 2015. Climate changes, lead pollution and soil erosion in south Greenland over the past 700 years. Quat. Res. 84, 159–173.
Steidtmann, J.R., Middleton, L.T., Shuster, M.W., 1989. Post-Laramide (Oligocene) uplift in the Wind River Range, Wyoming. Geology 17, 38–41.
Stone, J.O., 2000. Air pressure and cosmogenic isotope production. J. Geophys. Res. 105/B10 (23), 753–759.
Sun, H., Nelson, M., Chen, F., Husch, J., 2009. Soil mineral structural water loss during loss on ignition analyses. Can. J. Soil Sci. 89, 603–610. https://doi.org/10.4141/CJSS09007.
Viau, A.E., Ladd, M., Gajewski, K., 2012. The climate of North America during the last 2000 years reconstructed from pollen data. Glob. Planet. Chang. 84-85, 75–83. https://doi.org/10.1016/j.gloplacha.2011.09.010.
Whitlock, C., Briles, C.E., Fernandes, C.M., Gage, J., 2011. Holocene vegetation, fire and climate history of the Sawtooth Range, central Idaho, USA. Quat. Res. 75, 114–124.
Yu, Z., Eicher, U., 2019. Abrupt climate Oscillations during the last deglaciation in Central America. Science 282, 2235–2238.